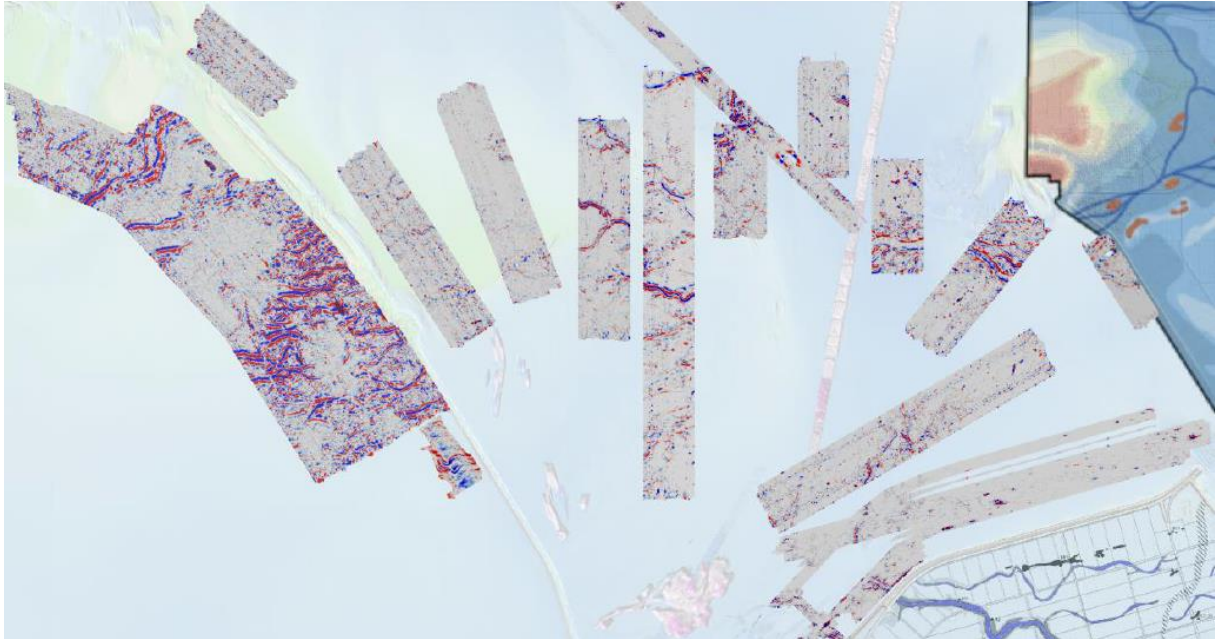# Magnetic Lineations in the Lake IJssel

Warner van Aalst 6297366

MSc Thesis

Supervised by dr. Mark Dekkers and dr. Kim Cohen

September 2022

Universiteit Utrecht

Faculty of Geosciences

Source cover photo: Overview of the recorded sub-bottom magnetic anomalies (van Lil & van den Brenk, 2021).

Abstract

In 2020, Periplus Archeomare was commissioned by de Rijksdienst voor het Cultureel Erfgoed (Cultural Heritage Agency of the Netherlands) to magnetically map the Lake IJssel (The Netherlands). Subsequent processing of this data resulted in the discovery of curvy-linear magnetic structures, reminiscent of gullies. It is our aim to discover the origin and elucidate the genesis of the positive/negative magnetic anomalies using paleomagnetic and rock magnetic methods. If the strata are paleomagnetically well behaved they could be dated paleomagnetically. Cores were sampled from a cross section of both positive as well as negative anomalies in a presumed river structure. The three sampled cores, VC15 of 5 meters, VC17 of 5 meters, and VC26 of 7 meters, contain the geologic history from the late Pleistocene to present of the Lake IJssel. Its geological make up consists, from the bottom up, of terrestrial – riverine – lacustrine – deltaic – lacustrine deposits. Magnetic susceptibility measurements indicate a stronger magnetic signal in the core segments containing clays. Acquisition curves of the isothermal remanent magnetization (IRM) and thermomagnetic analysis of the same strata show that the magnetic carrier is greigite (Fe_3S_4), diagentic in origin. The stratigraphic units in which greigite was primarily found are the Velsen Bed and Wormer Member. These are coastal deposits, or lacustrine/estuarine, allowing for an anoxic, sulfate reducing environment in which greigite can be formed. The influx of riverine freshwater of the Oer-Vecht and Oer-IJssel lowers the sulfate concentration in the water, and limits the reaction, allowing the preservation of greigite. The natural remanent magnetization (NRM) yielded interpretable trends from considerable portions of the cores. These trends however cannot be correlated faithfully to master curves of the paleosecular variation. Additional data points and age markers would allow to compare the Lake IJssel record to the paleomagnetic data sets of Western Europe.

Contents

1. Introduction

The Lake IJssel (IJsselmeer)is a former sea inlet, the Zuiderzee (Southern Sea), closed by the construction of the storm surge barrier dam Afsluitdijk (1932) (Fig. 1), in response to major flooding in the region in the 1910s. At the time construction of the Afsluitdijk was the biggest water-works construction worldwide. In a densely populated area, the Netherlands, sand for construction purposes is precious and the IJsselmeer contains a substantial amount (Van Den Brenk & Van Lil, 2017). In 2020, Periplus Archeomare was commissioned by de Rijksdienst voor het Cultureel Erfgoed to detect possible remnants of ships, aircraft, and bombs in the IJsselmeer, using side scan sonar, magnetometer and a single beam echo sounder.

Figure 1 The location of the Wadden Sea, the IJsselmeer (Lake IJssel), the Afsluitdijk, the river Vecht, and the river IJssel in the Netherlands. Adapted from Zandvoort et al., (2019).

Evidently, if present, their positions must be known in relation to harvesting sand from the lake for construction purposes. Subsequent processing of this data resulted in the discovery of linear magnetic structures, reminiscent of gullies. Comparable gully-like magnetic structures were discovered soon afterward near Urk and the northeast of Flevoland (Figure 2). During bathymetric research, via subbottom profiling and coring, it was found that these magnetic structures were located relatively deep (up to 10 m) in the subsurface. The magnetic structures have a width of up to 80 meters and can stretch up to several kilometers long (van den Brenk & van Lil, 2020; van Lil & van den Brenk, 2021). The current consensus is that the discovered lineations are buried remnants of ancient river systems (van den Brenk & van Lil, 2020; van Lil & van den Brenk, 2021). It is our aim to discover the origin and elucidate the genesis of the positive/negative magnetic anomalies, and, so ideally, contribute to the paleomagnetic secular variation data set of the Holocene in western Europe.
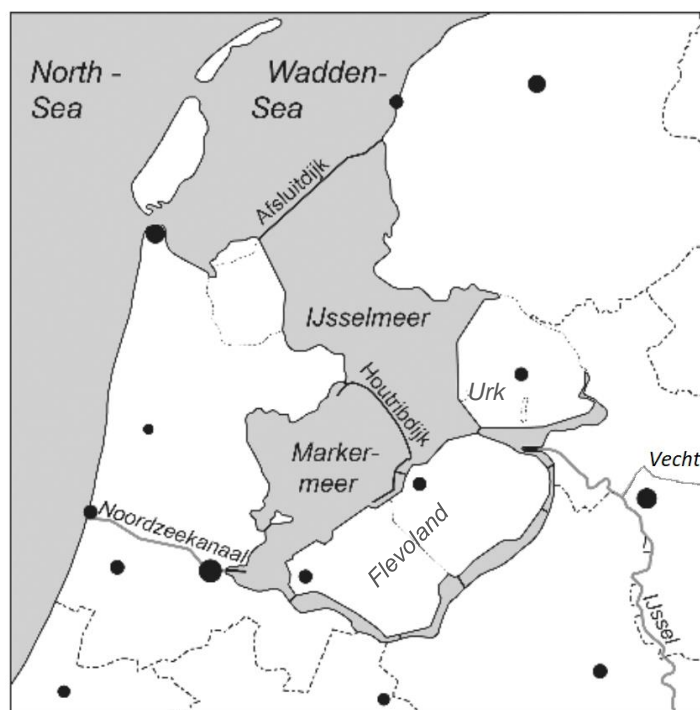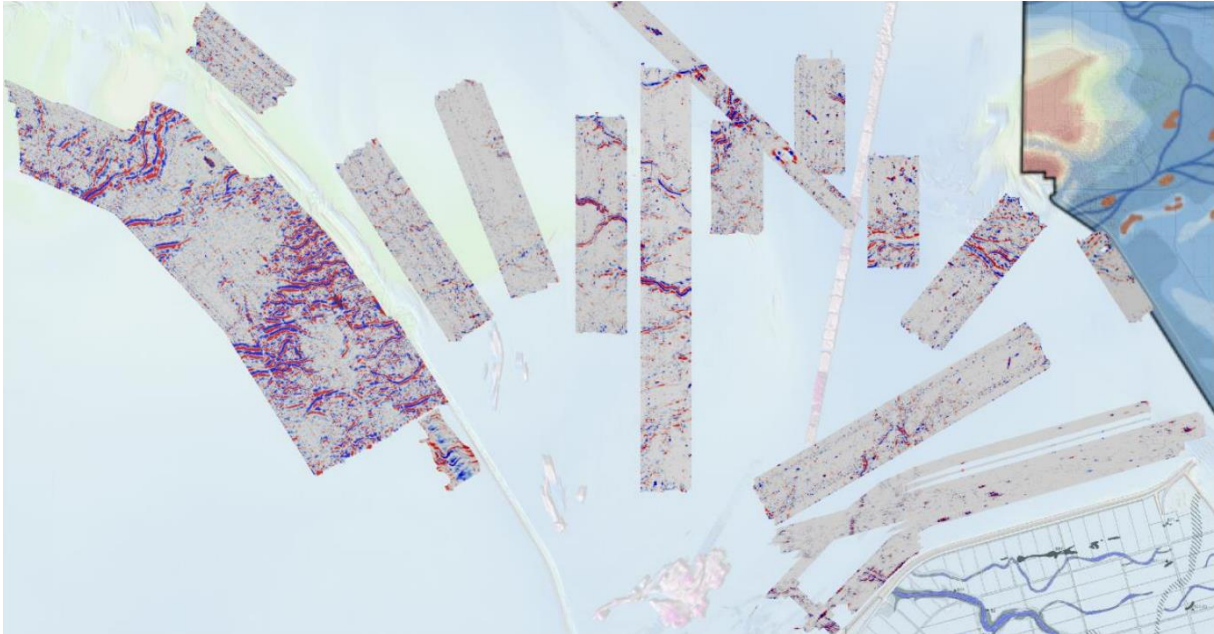
Figure 2: Overview of the magnetic lineations in the Lake IJssel (van den Brenk & van Lil, 2020)

1.1 Geologic History of the Lake IJssel

As mentioned before, the area of interest is the Lake IJssel and Markermeer (Lake Marken) region in the Netherlands. This area has a rich history in the recent geological past, a history at play when interested in the subsurface. The three collected cores, varying in length from 5.2 to 6.9 meters, reach back down to the Pleistocene and span the whole of the Holocene (11.7 kyr) (van den Brenk & van Lil, 2020; van Lil & van den Brenk, 2021; Walker, 2019). The different layers in are deposited during different times and of different facies within the Holocene. The Holocene began about 11.700 years ago and continues till today/the present. The climate began to stabilize in the form of an interglacial. At the start of the Holocene the sea level had risen to about 60 meters -NAP, compared to the present day level (Smith et al., 2011). Most of the Netherlands has been formed during the Holocene. The geology of the Netherlands is formed by the sea and rivers, and thus highly susceptible to sea level, and thereby climate (Stouthamer, 2015; Vos, 2015). The Holocene starts with a temperature rise to current values, coinciding with the melting of the northern ice caps and subsequent sea-level rise (Carlson & Clark, 2012). Figure 3 gives an overview of the Holocene periods covered in this study.
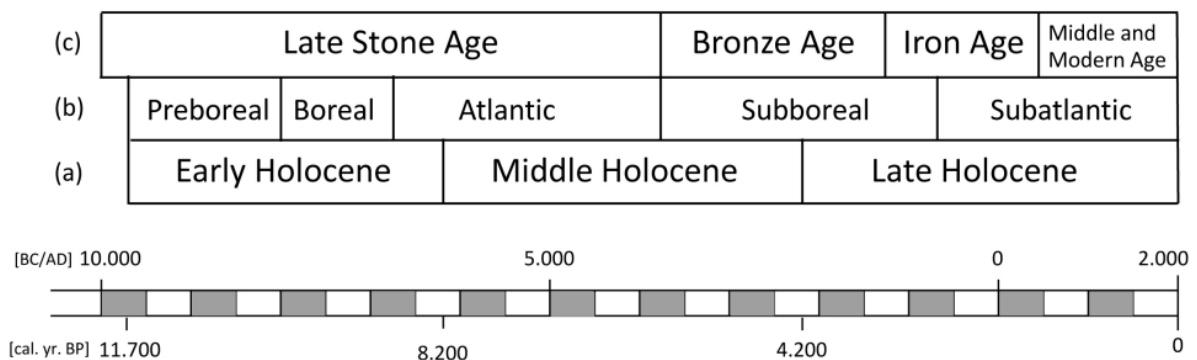

Figure 3: Holocene subdivisions, temporal range and human history periods. Cal. Yr. BP refers to calibrated years from present, with the present being the year 2000 (Čalasan et al., 2019).

While the subsurface touched upon in this research is primarily formed during the Holocene, the conditions allowing for these facies find their origin in pre-Holocene times. The morphology of the subsurface is created during the Saalian (238 – 126 ka) Here, the Overijsselse Oer-Vecht Valley is formed, at that time being the course of the Rhine river (Busschers, 2008). This valley is what will shape the morphology of the Zuiderzee area. The ensuing Eemian interglacial (126 – 116 ka), and Weichselian glacial (116 – 11.70 ka) allowed for the deposition of marine and terrestrial material (Westerhoff et al., 1987). During the Early Holocene, the Overijsselse Vecht watershed compromised the eastern Netherlands and parts of Germany(Busschers, 2008). At the time the sea level was about 35m -NAP, i.e. 35m lower than today. The present-day Dutch coast and large parts of the southern North Sea were dry ground (cf. Beets & Van der Spek, 2000). Figure 4 offers a birds-eye view of how the Netherlands developed from the early Holocene till now. We discuss it next.

With the start of the Atlanticum (8000 yr BP, Fig. 4 a), a major climate shift takes place. The sudden outflow of meltwater from glacier lakes caused an abrupt rise in sea level and the start of coastal and delta deposition in the Netherlands (Stouthamer, 2015; Vos, 2015; Jelgersma, 1996; Van de Plassche, 1982; Kiden, 2002). In the primeval valley of the Overijsselse Oer-Vecht, the water table is raised, and on top of the Pleistocene sand deposits, peatlands start to form. The Basal Peat (Basisveen) formation comes into being. The formation of this peat layer was the effect of rising groundwater levels, up to, or just above ground level, in combination with seepage water discharged from the Pleistocene sand deposits (Berendsen, 2005; Vos, 2015; Güray, 1952). The Western Netherlands changes into a large landward-expanding open-water tidal basin, connected to the North Sea via multiple tidal inlets (Beets et al., 1994) (Fig. 4 a). It is in this area that the Wormer Member (Laag van Wormer) starts being deposited.

Continued sea level rise (25 to 20 m -NAP) flooded the lower peat marshes in the paleovalley at around 7500 BC and the Basal Peat became covered with the lagoonal clays of the Velsen Bed (Laag van Velsen). Around 6500 BC the southern and northern halves of the North Sea became connected, attaining its present-day size. The deepening of the North Sea and other changes in its bathymetry eventuated an increase in tidal amplitude along the Dutch coast (Van der Molen & De Swart, 2001; Hijma & Cohen, 2011), with effects reaching the former Oer-Vecht valley. In the Overijsselse Oer-Vecht system, now drowning, these forces allowed for the creation of large tidal channels. The high pace of the sea level rise outran sedimentation and an embayment developed, as well as tidal flats and tidal channels towards the landward basin margin (Fig. 4 b).

At about 3850 BC (Fig. 4 c) the tidal basin that is the Overijsselse Oer-Vecht has expanded to its maximum size, covering almost all of present-day Flevoland (Ente, 1986; Lenselink & Koopstra, 1994). Hereafter, sedimentation start to overtake sea level rise, exceeding accommodation space, and sediments from the sea and rivers silt up the tidal basin (Van der Spek, 1994, Beets & Van der Spek, 2000). The wet area of the tidal inlet decreased (Oost & De Boer, 1994), and the landward migration of the shoreline was reversed. In the hinterland, salt marshes start to form (Vos & De Wolf, 1988, 1994).

In 3200 and 2500 BC (Fig. 4 d), the hinterland became waterlogged as a consequence of the decreased drainage caused by the silting up of the tidal channels. This allowed for large-scale peat development, isolating the central parts completely from the nutrient-rich sea waters. Oligotrophic peat formation and accumulation takes place in these areas.

After 2750 BC (Fig. 4 d) the lake IJssel area drainage works through the large Westfriese inlet system, being the main remnant of the Oer-Vecht tidal basin (Lenselink & Koopstra, 1994). The propagation of the coastline continues with the regression of the sea level and even accelerates, decreasing marine influence in the hinterland.

At around 1500 BC (Fig. 4 e) the Westfriese inlet silted up, closing off the tidal basin from the sea completely (Roep et al., 1979; Beets et al., 1996) (Fig. 4 e) Unable to drain, the groundwater started to rise, and peat lands start to form again, at the cost of salt marshes.

These peat marshes form the Hollandveen Bed (Berendsen, 2005; Vos, 2015; Güray, 1952). During intrusion of the sea via the Oer-IJ and from West-Friesland, parts of the Hollandveen were eroded and inlets were created, eventually forming lakes. Formation of new peat in these inlets created the Flevomeer Bed.

At about 800 BC the Rhine River connected with the Utrechtse Vecht system, when the peat lakes in the Vecht region became interconnected. This created a continuous waterway between the Rhine and the Flevo Lakes and resulted in the deposition of Rhine River sediments in the Flevo Lakes (Bos, 2010). This system drained via the Oer-IJ in the North Sea. The Overijsselse Vecht and the northern Flevo Lakes drained via a separate outlet in the Wadden Sea (Fig. 4 f). In 400 BC the northern and southern Flevo lakes connect, resulting in the silting up of the Oer-IJ tidal area. The Flevo Lakes and the Utrechtse Vecht region now discharge via the Wadden Sea.

The lakes in this area continued to grow via coastal erosion and during the Middle Ages, it created the central Lake Almere, continuing to exist until 1250 AD (Fig. 4 g, h). The water in the Almere Lake turned brackish, brought about by the influx of sea water. Eventually, a connection with the Waddenzee, and thus the North Sea, was restored and the waters turned more saline (Figs 4 I - J). The former lakes became known as the Southern Sea (Zuiderzee) (Pons & Wiggers, 1960). A layer of sea clay was deposited, ranging in texture from clay to sandy, named the Zuiderzee Layer. In the IJssel delta calcareous sediments were also deposited at this time (Berendsen, 2005).

From 1850 (Fig. 4 j) man started to become a geological factor to take into consideration. Large scale land reclamation processes took place and peat lands were made dry, yet flood risk were still high and dikes were often breached. As the urbanisation of the Netherlands continued and to counteract storm floods, large land reclamations took place. The Afsluitdijk was constructed closing off the Zuiderzee in 1932 and creating the Lake IJssel (Fig. 4 k) (Vos, 2015).The genesis and morphology of the IJsselmeer area are thus heavily influenced by the interplay of the rivers and sea.
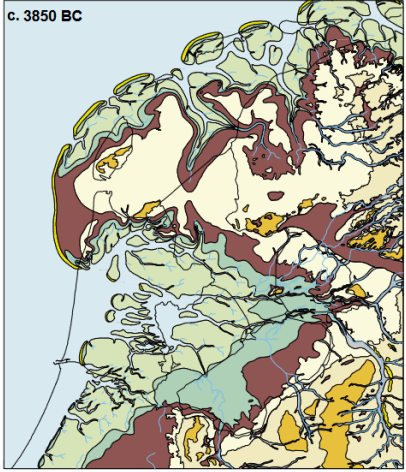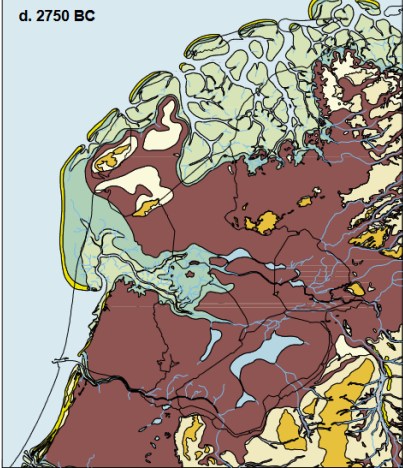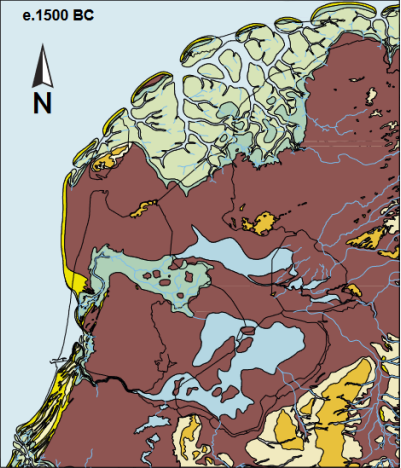
a. 9000 BC

N
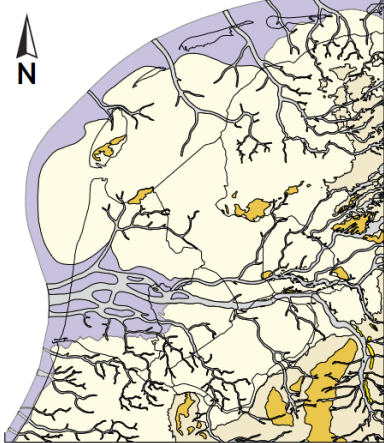
b. 5500 BC

c. 3850 BC

d. 2750 BC

e. 1500 BC

N

f. 500 BC
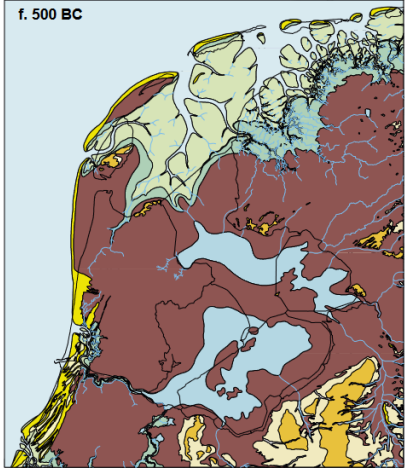
g. 100 AD

h. 800 AD

i. 1500 AD

N

j. 1850 AD

k. 2000 AD

9
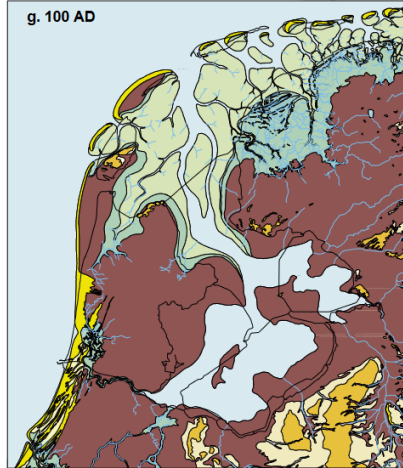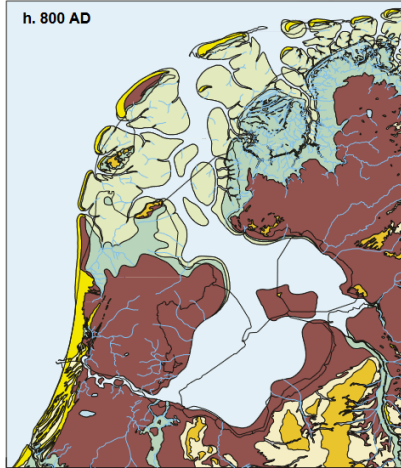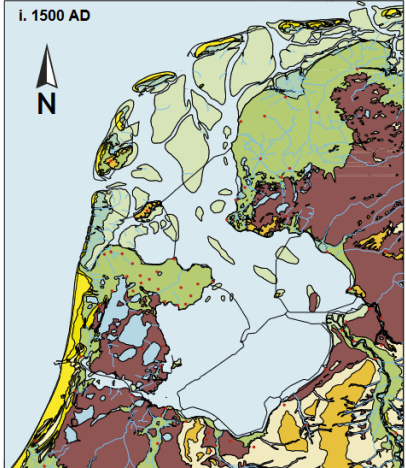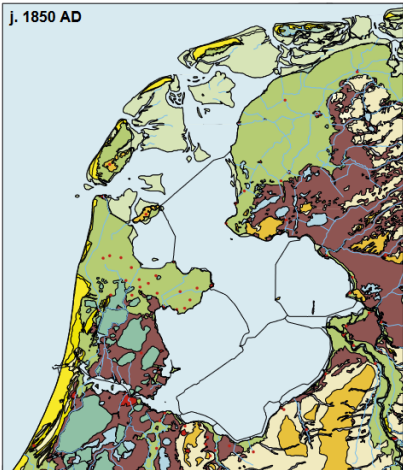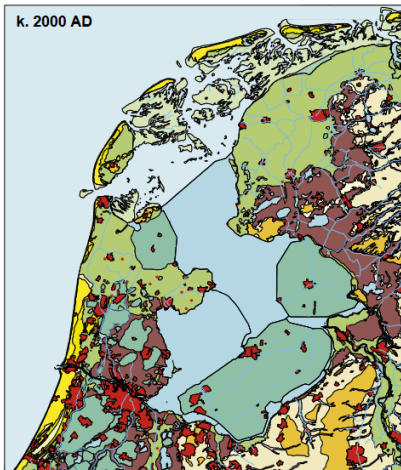
Holocene landscape

Coastal dunes

Dunes and beach ridges

Flooded areas

Intertidal areas: sand- and mudflats

Fluvial flood plain and marine salt-marsh area

Salt-marsh levees and ridges: relative high parts in the salt-marsh area

Peat areas

Peatlands

Anthropogenically created areas

Embanked / reclaimed areas

Former lakes (pumped dry)

Urban areas

Permanently submerged water areas

Non-tidal waters: mainly freshwater features such as, river channels and lakes
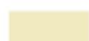
Tidal waters: mainly brackish and marin

Pleistocene landscape

River and brook valleys

Pleistocene sand areas, below 16 m -NAP and presently buried

Pleistocene sand areas, between16 en 0 m –NAP and presently buried

Pleistocene sand areas, above 0 m –NAP

River dunes ("donken")

Pushed moraines and drumlinss

Symbols

—— Coastline

—— Creeks, streams and waterways

• Cities

Figure 4: Paleogeographical maps of the northwestern Netherlands between 9000 BC and present (Vos et al. 2015).

1.2 Substrate & Sampling

12.1 Substrate

The sedimentary stratigraphy is divided hierarchically into formations, members, and beds, as displayed in Table 1. In the longest core of 6.20 meters sediments originating from the Pleistocene are also present. The distinguished stratigraphic units are lithostratigraphic, implying that they are not uniformly present in space and time. The Drenthe Formation consisting of glacial deposits is present in the form of the Gieten member. This member consists of subglacial deposits ranging from clay and loam to gravel up to boulder size (*TNO-GDN (2022). Gieten Member).* It has a sharp contact with the superposed Boxtel Formation. This formation takes form in periglacial aeolian deposits, such as coversands. In the research area, it may have been subjected to gelifluxion (van Lil & van den Brenk, 2021). Its upper boundary is characterized by an erosive contact with the Naaldwijk Formation (*TNO-GDN (2022). Formatie van Boxtel)*

The Holocene coastal deposits are lithostratigraphically (not chronostratigraphically) divided into two formations. The Naaldwijk Formation (NaF) contains clastic coastal deposits, such as dunes, beaches, and tidal facies (Westerhoff et al., 2003). The Nieuwkoop Formation (NiF) consists of organic depositions accumulated in coastal-peat bogs (Doppert, 1975; Westerhoff , 2003; *TNO-GDN (2022). Formatie van Naaldwijk.*). The Holocene depositis are often underlain by the Basal Peat (Basisveen, NiF), a peat layer directly on top of the Pleistocene substrate at the base of the Holocene coastal sequence (Doppert, 1975; Westerhoff , 2003; *TNO-GDN (2022). Formatie van Naaldwijk.*). However, this may be out of the reach of the core intervals.

The lowest Holocene layer found belongs to the Wormer Member (Laagpakket van Wormer, NaF). This is the Velsen Bed (Laag van Velsen, NaF), consisting of humic and lagoonal clays (Bennema, 1954; *TNO-GDN (2022). Laag van Velsen.*). The Wormer Member itself, situated on top, composes a tidal deposit between the Basal Peat and the Hollandveen Member (*TNO-GDN (2022). Laagpakket van Wormer*). Superposed is the Hollandveen Member (*TNO-GDN (2022). Hollandveen Laagpakket.*), a peat layer underlain by the Holocene clastic tidal deposits. Next is the Flevomeer Bed (*TNO-GDN (2022). Flevomeer Laag*). A mixed sediment and disintegrated peat layer on top of the Hollandveen Member (NiF) (Weerts & Busschers, 2003; Zagwijn & Van Staalduinen, 1975). The Walcheren Member (*TNO-GDN (2022). Laagpakket van Walcheren*) is defined as containing tidal deposits above the uppermost Hollandveen Member layer or Basal Peat. Within the Walcheren Member the Almere Bed (*TNO-GDN (2022). Almere Laag.*can be found, located above the Flevomeer Bed. Consisting of lagoonal clay and detritus and forms a sharp boundary with the Nieuwkoop Formation. On top the Zuiderzee Bed (*TNO-GDN (2022). Zuiderzee Laag.*), consits of tidal sediments, as clay and fine sand. It forms a sharp contrast with the lagoonal clays (Almere Bed) found below it (Weerts, 2003).

Serie	Formation	Member	Bed	Lithology
Holocene	Naaldwijk Formation	Wormer Member	Velsen Bed	Clay, organic, laminated, rooted with reeds. Insertions of silt, sand and organic detritus laminae. Upwards increase of fine sand and decrease in organics.
		Walcheren Member	Almere Bed	Clay, detritus, and silt. Distincly layered with very fine to medium sand.
			Zuiderzee Bed	Fine sand, clayey, calcareous, silty, shelly. Alternations of sand-clay. Bioturbation.
	Nieuwkoop Formation		Basal Peat	Compact peat with layers of gyttja. Locally clayey.
			Flevomeer Bed	Organoclastic detritus. Physically disintergrated peat, as well as slightly clayey. Gyttja with layers of silt and fine sand.
		Hollandveen Member		Gyttja and Peat. Fibric to amorphous structure. Found in situ as well as detrital.
Pleistocene	Boxtel Formation			Periglacial aeolian deposits, such as coversands. Possibly subjected to gelifluxion
	Drente Formation	Gieten Member		Subglacial deposits ranging from clay and loam to gravel up to boulder size

Table 1: Lithological overview of present lithostratigraphy (van den Brenk & van Lil, 2020; van Lil & van den Brenk, 2021; TNO-GDN (2022). Boven-Noordzee Groep *).*

1.2.2 Sampling

Magnetic measurements performed by Periplus Archeomare indicated gully-like magnetic structures in the subsurface of the IJsselmeer and Markermeer. These curvy-linear patterns seem to connect to the systems of the Overijsselse Oer-Vecht and Oer-IJssel. Bathymetric research indicated that these structures were located well in the subsurface. Subbottom profiling showed that they likely present covered gullies. Magnetic scanning of the area is shown in figure 5. Based on these scans and subbottom profiling vibro cores reaching a depth of -8.4 to -9.4 m NAP were taken. A lithostratigraphic profile was made based on the cores taken (Fig. 6).

Figure 5: Core locations section D. Red indicates a positive anomaly, while blue indicates a negative anomaly (van Lil & van den Brenk, 2021).

In section D (Figure 6), cores VC15 (positive anomaly) and VC17 (negative anomaly) are selected for research. These cores offer a transect of layers deposited during the Holocene and the subsequent history of gradual drowning of the river gullies by a rising sea level (van den Brenk & van Lil, 2020; van Lil &
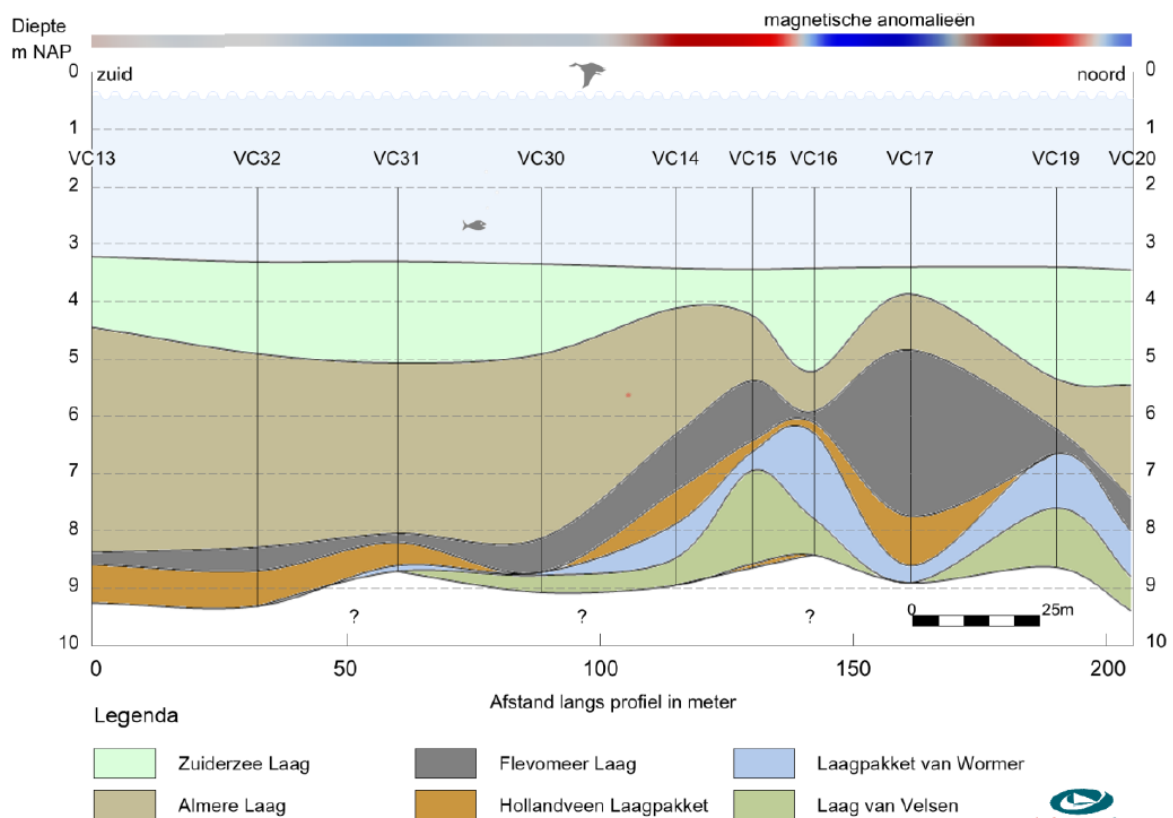
Figure 6: Lithostratigraphic profile of section D, positive magnetic anomalies (red) and negative magnetic anomalies (blue) (van Lil & van den Brenk, 2021).

van den Brenk, 2021). While magnetite is a common cause for magnetic anomalies, the

depositional environment under study allows for the formation of another magnetic mineral. Greigite (Fe_3S_4) could form in this setting and be a possible explanation for the magnetic anomalies.

Conversely, Section E (Fig. 7) offers a transect of layers up to the Pleistocene. The magnetic signal shows a different pattern in relation to the stratigraphy compared to section D. The central river system is a negative magnetic anomaly and the outer banks are positive. Potentially, a different component is the cause of the magnetic signal at this location. To test this idea, core VC26 (Fig. 8), featuring a negative anomaly, reaching till the Pleistocene shall be sampled.
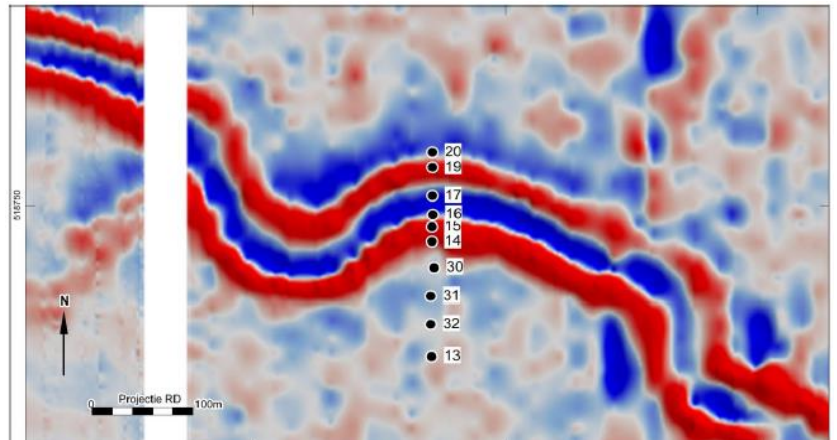

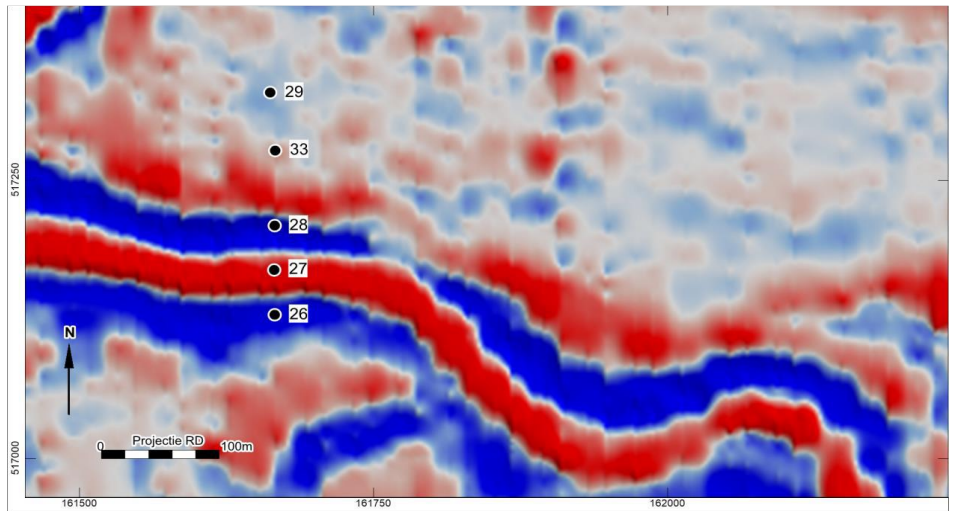*Figure 7: Core locations of section E. Red indicates a positive anomaly, while blue indicates a negative anomaly (van Lil & van den Brenk, 2021).*
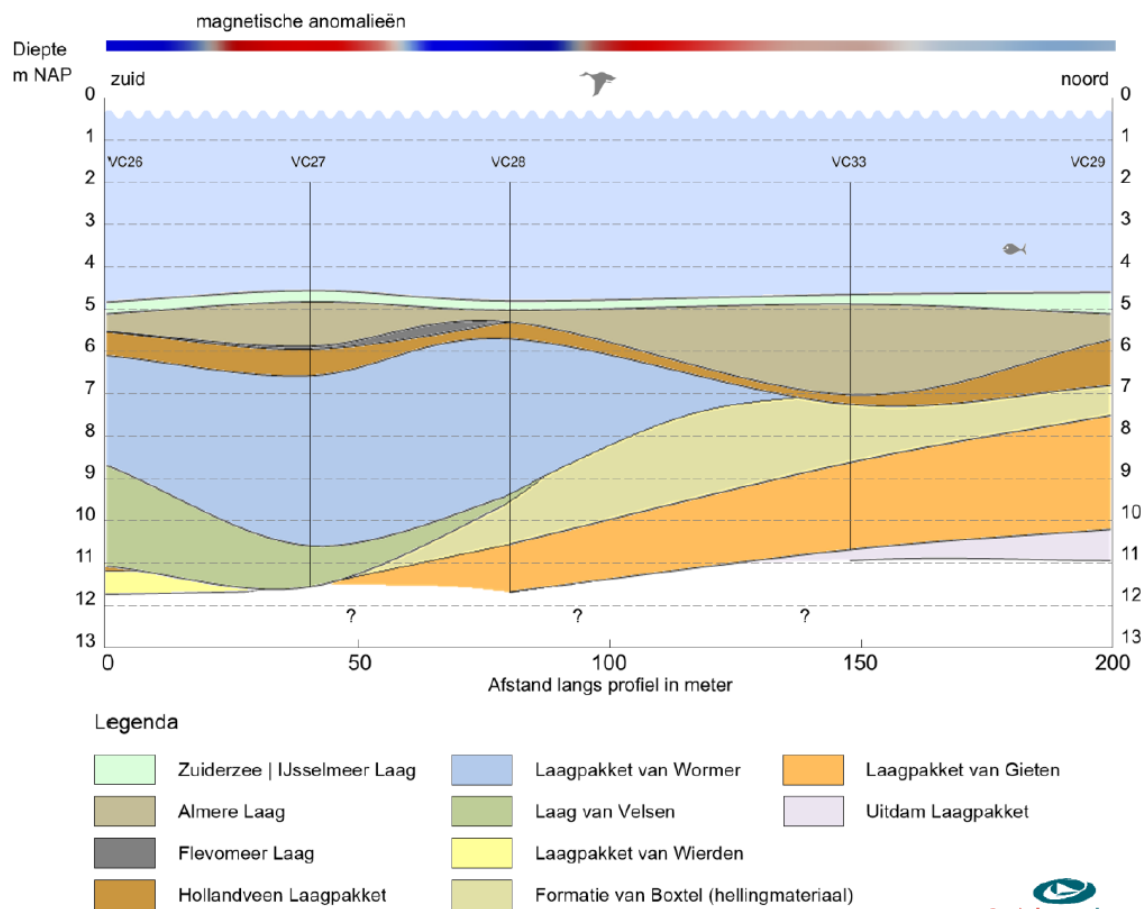
Figure 8: Lithostratigraphical profile of section E, with magnetic anomalies (van Lil & van den Brenk, 2021).

14

Based on magnetic susceptibility measurements sampling intervals were determined. Core VC15 was sampled with a 10 cm interval for the low susceptibility portion, while the high susceptibility parts were sampled with a 7 cm interval. The whole core VC17 showed low susceptibility and thus was sampled with an interval of 15 cm. Core VC26 was sampled with a 15 cm interval for the low susceptibility parts and an interval of 10 cm for the high susceptibility parts.

1.3 Magnetic minerals and depositional environment

The discipline of paleomagnetism focuses on the permanent magnetic moments or remanent magnetizations stored in rocks as a function of space and time. It studies primarily the directional information recorded in the rocks although increasingly also studies into the paleointensity (the strength of the past geomagnetic field) are being undertaken. The paleomagnetic signal is stored in magnetic minerals in a rock or sediment sample. The natural magnetic minerals are comprised mainly of oxides and sulfides of iron. The most important terrestrial magnetic mineral is magnetite (Fe_3O_4). This permanent or remanent magnetic signal finds its origin in the atomic scale, as a result of the uncompensated spin moment of the outermost electrons orbiting around the nucleus. While these spin moments generally cancel out in crystalline solids, this is not always the case. Crystalline solids with overlapping orbits of the outermost electrons have uncompensated spins that line up, and consequently have a summation of individual magnetic moments into a macroscopic magnetic moment (Dekkers, 1997).

The previous research by van den Brenk & van Lil, 2020 and van Lil & van den Brenk, 2021 indicates that the Lake IJssel lithology consists of lagoonal and swampy environments. These environments are often anoxic and sulfate-reducing (Roberts et al., 2011b). It is hypothesized that the origin of the magnetic anomalies found in the Lake IJssel is sedimentary greigite (Fe_3S_4), rather than the more common magnetite (Fe_3O_4). Multiple studies report the presence of greigite in both freshwater as well as marine environments (Kelder et al., 2018; Sant et al., 2018; Snowball & Thompson, 1990; Vasiliev et al., 2008).

Greigite is a strongly ferrimagnetic iron sulfide (Chang et al., 2014) with specific environmental and paleomagnetic properties and forms in aquatic anoxic sedimentary environments. There are several ways for greigite to form. Amongst them is that greigite is a precursor to pyrite (FeS_2), an intermediate phase in the pyrite formation reaction chain. The formation of greigite is dependent on the availability of sulfide, organic carbon, and concentration of reactive iron. Sulfate reduction happens as a biologically induced enzymatic reaction; for pyrite formation (and its precursors) the iron detaches from silicates and pore water sulfate is the source of sulfide. The conversion to pyrite can be halted when reactive iron is abundant and dissolved sulfide concentrations are low (Kao et al., 2004; Berner & Baldwin, 1979).

Another possibility of greigite formation besides being formed diagenetically, is that greigite can also have a biological origin. Sulfidic magnetotactic bacteria (MTB) produce greigite crystals intracellularly as a biological compass, allowing them to navigate along the magnetic field lines (Bazylinski & Frankel, 2004; Farina et al., 1990; Mann et al., 1990). There are several hypotheses as to why magnetotactic bacteria produce magnetosomes. MTB generally live in the sediments in sulfate-reducing conditions below the oxic-anoxic interface. The most common hypothesis is that it allows the bacteria to be passively orientated by the magnetic field, which has a vertical component in the northern and southern hemispheres, directed from or towards the surface (Frankel & Bazylinski, 2006). A one-directional active motion is energy-wise advantageous over the three-dimensional random motions that non-magnetotactic organisms have to perform to arrive in their optimal habitat (Klumpp et al.,

2019). However, considering that there are also MTB at the equator, where there is no vertical magnetic field component (Frankel et al., 1981), and as it turns out, these creatures do not always live in the sediments, it is also suggested that magnetosomes could have additional functions as energy storage (Byrne et al., 2015).

The preserved remains of these bacteria are called magnetofossils and form a valuable contribution to the paleomagnetic record and can be indicative of environmental processes (Chang et al., 2013; Heslop et al., 2013; Yamazaki, 2012). Paleomagnetic greigite records can be difficult to interpret. Diagenetic greigite can form postdepositionally, allowing for a time lag with stratigraphy, and potential remagnetization (e.g. Sagnotti et al., 2010), deeming it as unreliable for paleomagnetic studies for a long time. However, increased understanding of the formation of greigite has allowed for the discovery that MTB-produced greigite carries a syndepositional magnetic signal, and can be used for paleomagnetic interpretations (Chang et al., 2014; van Baak et al., 2016; Vasiliev et al., 2008). This gives the potential for reliable paleomagnetic signals to be obtained from greigite-bearing sediments when proper demagnetization methods are followed (Kelder et al., 2018).

In this study magnetostratigraphic results are presented from 3 cores of the Lake IJssel, covering the upper boundary of the Pleistocene till Holocene. This is done to assess the origin and formation of the magnetic lineations. In order to study this case, rock magnetic techniques are used incorporating thermal and alternating field demagnetization.

2. Methods

Paleomagnetic and magnetic property measurements were performed at the Paleomagnetic Laboratory 'Fort Hoofddijk' at Utrecht University (The Netherlands).

2.1 Rock Magnetic Analyses: Magnetic Susceptibility

Magnetic susceptibility measurements were performed on the cores in ambient temperatures using the SM-30, a handheld susceptibility meter, with a sensitivity of $1*10^{-7}$ SI units. The noise produced in the pick-up coil is lower than $1*10^{-7}$ SI units 1 (SM_30, n.d., p. 30). A small magnetic field is applied, interacting with the sediments in the core. Differences in susceptibility are an indication of varying magnetic composition and/or concentration of the magnetic components in the sediments (e.g. Béguin et al., 2019; Dunlop & Özdemir, 1997; Evans & Heller, 2003). The cores were screened with an interval of 5 cm, and the results were used to construct a detailed sampling plan.

2.2 Rock Magnetic Analyses: Thermomagnetic Analysis

The magnetization versus temperature of semi-dried powdered samples was measured in air by a modified horizontal translation-type Curie balance, using a sinusoidally cycling applied magnetic field. This device has a sensitivity of ~5×10^{-9} Am^2 (Mullender et al., 1993). The powdered sample was placed in a diamagnetic quartz holder and was subjected to a magnetic field in a small area, creating a strong field gradient. The paramagnetic and ferromagnetic particles within the sample are attracted towards the stronger magnetic field, while the diamagnetic particles are repulsed. The current necessary to create an opposite force of comparable strength, by a compensation coil, to keep the rod with the sample at the same

position is proportional to the magnetization of the sample in the external field (Collinson, 1983; Fabian et al., 2013). All the while, the samples were heated and cooled in a stepwise fashion at rates of 6 and 10°C/min. The peak temperatures of the successive cycles were 150, 250, 400, 520, 620, and 700°C, respectively (Yang et al., 2018). In between the maximum temperatures the samples were cooled by a 100°C lower than the maximum temperature of each cycle, to see whether the magnetic signal deviated. If that occurs, it indicates thermochemical alteration. The Curie temperatures of the samples are derived by the two-tangent method developed by Grommé et al., (1969).

2.3 Rock Magnetic Analyses: Isothermal Remanent Magnetization

Of all samples, acquisition curves of isothermal remanent magnetization (IRM) were constructed, using 42 acquisition steps up to 700 mT. Measurements were performed on a Long-core version of the superconducting rock magnetometer Model 755 HR. This device consists of three orthogonal DC-SQUIDs and three orthogonal coils for alternating field demagnetization. The sensing region of the pickup coils of the SQUIDs and AF coils ideally have a residual field intensity of <5nT in each direction inside the magnetic shielding. However, the residual field in the AF demagnetization unit is more likely to be around 300 nT (M. Dekkers, personal communication, August 15, 2022).

Furthermore, the instrument has an inline pulse magnetizer used for stepwise acquisition of Isothermal Remanent Magnetization (IRM). Depending on the bore size of the magnetometer, the practical maximum field is 700 mT. The samples are placed at distances of 20 cm on the sample tray, to avoid interference of the sample signals. This tray subsequently slides through the bore of the magnetometer (Mullender et al., 2016).

In IRM acquisition a magnetization direction parallel to the last demagnetization direction of the static three-axial-AF state is acquired. This ensures minimal deviation from lognormality for the low levels of anticipated magnetic interactions (Heslop et al., 2004).

The magnetic components present in these IRM acquisition curves were extracted using the IRM fitting program of Kruiver et al. (2001). This program allows for the characterization of magnetic components by cumulative log-Gaussian (CLG) functions, via three parameters: 1. The saturation IRM (SIRM), the magnetic concentration of the individual phase; 2. The field at which half of the SIRM is reached ($B_{1/2}$), indicative of the magnetic mineralogy and grain size; and 3. The width of the distribution: the dispersion parameter (DP), which is given by one standard deviation of the logarithmic distribution. This parameter provides information on the distribution of the grain size as well as potential crystal defects. The data is plotted in three different plots per sample. 1. The linear acquisition plot (LAP), 2. the gradient acquisition plot (GAP), and 3. the standardized acquisition plot (SAP). When using this method it is assumed that there is no magnetic interaction between different magnetic particles in a sample and that an IRM acquisition curve follows a cumulative Log-Gaussian function (Robertson & France, 1994). However, in reality, thermal activation and magnetic interaction do cause deviations from a true log-Gaussian distribution. This can however be accounted for in the subsequent data processing (e.g. Heslop et al., 2004). Generally, a small contribution and low $B_{1/2}$ in the first component are signs of thermal activation. This component should subsequently not be interpreted as a carrier of a magnetic signal (Egli, 2004).

2.4 Paleodirections: Normal Remanent Magnetization - Alternating Field demagnetization

Since the lithostratigraphic units that make up the research area are time independent in origin, a dating method is necessary to correlate these between cores. Paleomagnetic secular variation (PSV) is such a dating method. Here temporal variations in the magnetic field in time are studied, and used as a record (Johnson & McFadden, 2015).

The Natural Remanent Magnetization (NRM) of each sample was stepwise progressively demagnetized with alternating field (AF) demagnetization in fields up to 120.0 mT. Measurements were performed on a robotized DC-SQUID magnetometer. This set up has an in house produced computer interface. It has a sensitivity of $3*10^{-12}$ Am^2, which results in a sample magnetization of ~$3*10^{-7}$ Am^{-1} for a standard paleomagnetic sample of 10 cm^3 (Mullender et al., 2016).

The possible presence of greigite in the samples could lead to complications as greigite is prone to acquire a gyro-remanent magnetization, and thus create a biased demagnetization curve (Roberts et al., 2011b). This necessitated the use of the AF 'per component protocol' for AF demagnetization (Dankers & Zijderveld, 1981). In a zero-field environment, the AF is ramped to a certain value in three orthogonal directions and then slowly ramped down to zero, magnetically cleaning the sample. Only the component parallel to the last demagnetization axis is used to calculate the remaining NRM vector, meaning that the other components have to be AF demagnetized a second time to allow for the interpretation. The interpretation was done via paleomagnetism.org version 2 (Koymans et al., 2016, 2020), using the declination and inclination values obtained through Zijderveld diagrams (Zijderveld, 1967) with unanchored fits, as according to Heslop & Roberts (2016) anchoring creates a statistically unsound elongation of the covariance structure of paleomagnetic data. A minimum of 4 consecutive steps between the AF-levels of 20 to 85 mT were utilized as criteria. Samples with a Maximum Angle of Deviation (MAD), a measure of uncertainty, greater than 7° in an unanchored fit were rejected. Considering that the cores were not azimuthally oriented when taken from the Lake IJssel, the constructed declination records are relative in nature. This is done by so by setting the average declination per core segment to zero. Considering the small time interval the core segments contain and small data density, results from this method should be used cautiously.

2.5 Relative Paleointensity: Pseudo-Thellier

In order to retrieve the relative paleointensity, the relative strength of the magnetic field in the past, the Pseudo-Thellier method by Tauxe et al. (1995) was applied. Pseudo-Thellier experiments consist of three steps (de Groot et al., 2013), in which the NRM, ARM acquisition, and ARM demagnetization are combined, using the same field steps. After the NRM demagnetization, when the AF goes from peak value to zero, Anhysteretic Remanent Magnetization (ARM) is applied to the samples at the same field levels as the NRM demagnetization. This results in an ARM acquisition curve. A direct current (DC) bias field equivalent to a field of 40 µT is superposed on an AF of a given strength which induces a remanent magnetization, termed ARM. The maximum ARM in the samples was stepwise demagnetized in the same intervals as the NRM (and ARM acquisition), in order to compare the affected grains. ARM measurements were performed on the robotized 2G DC-SQUID

magnetometer. The Pseudo-Thellier technique compares the demagnetized NRM and the acquired ARM for increasingly higher AF values in an Arai plot (figure 9).

The intensity of the remaining NRM after imparting the demagnetization field is plotted on the vertical axis against the intensity of the ARM acquired in the same field on the horizontal axis. The now visible line in the Arai plot can be fitted (Fig. 9). If the plotted data
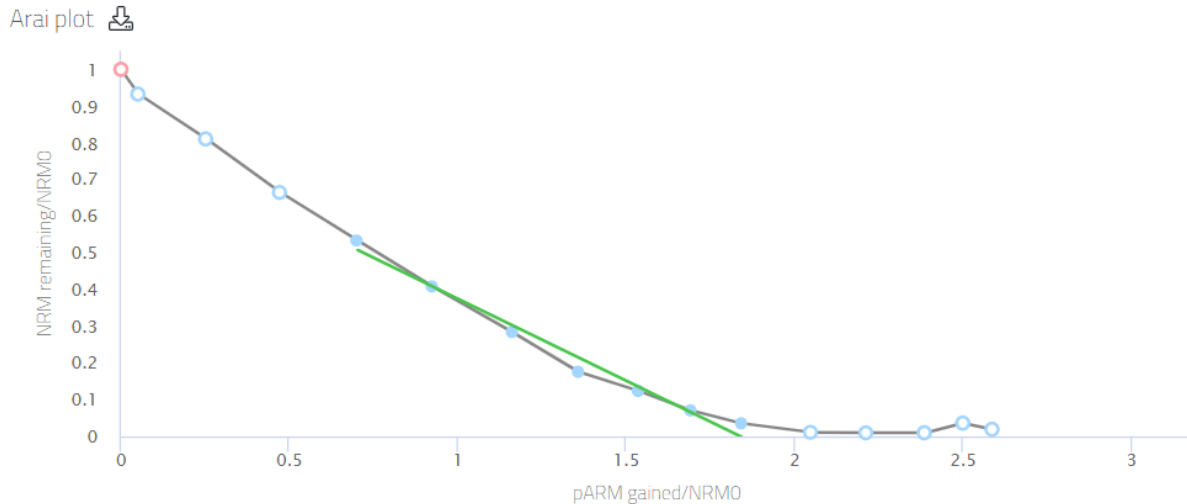
Figure 9: Arai plot, with a selection of points creating a linear fit (green line) (Béguin et al., 2020).

behaves proportionally, a linear fit is visible and indicates that the grains carrying the demagnetized NRM are the same grains carrying the acquired ARM. The slope of this fit is a measure of the intensity between these fields. Since the same bias field was used for all samples, the pseudo-Thellier slope can be used as a relative indicator of paleointensity.

The pseudo-Thellier data was analyzed using paleointensity.org (Béguin et al., 2020). The data below 10 mT is deemed unreliable and often deviates from the linear fit. A selection of fields between 15-100 mT are used to obtain the slope of the linear fit.

2.6 Elemental analyses: X-Ray Fluorescence

Changes in the elemental composition of the cores was measured with a handheld Thermo Scientific Niton XL3t XRF Analyzer, by analyzing X-ray fluorescence (XRF). Measurements were performed on the flat surface of the cores, in the open air, at ambient temperatures. Intervals of 10 cm were used. Due to the lack to a standard to calibrate to, found trends are primarily to be considered as relative to each other and not absolute. Elements which were usable in the circumstances the device operated were Rb and Sr.

3. Results

3.1 Magnetic susceptibility

In figure 10 the magnetic susceptibility of the three cores is plotted against depth. Between the cores, a clear difference is visible in terms of susceptibility magnitude. The core VC17 (Fig. 10 B) shows values being about 10^{-2} SI volume units, while VC15 and VC26 (Fig. 10 A, C) are in the range of 10^{+1} SI volume units. The trends in the susceptibility measurements seem to be dominated by paramagnetic or ferromagnetic minerals. Diamagnetic measurements do occur but are only a few. A difference in formations and composition in terms of depth is also discernable between the cores. Highlighted in blue and light green are the Wormer Member and Velsen Bed (Fig. 10 A, C), the sections of the cores having high susceptibility measurements. These beds are mostly comprised of clay, as a result of being deposited in a brackish environment. Core VC17 lacks high susceptibility measurements and contains few clay beds either. An interesting observation is that the clayey parts of the core have white crystals forming on the surface, the size of fine sand grains. These crystals were interpreted to be vivianite $Fe^{2+}_3(PO_4)_2 \bullet 8(H_2O)$ (K. Cohen, personal communication, December 17, 2021)

A

VC15

B

VC17

C

VC26

Depth in cm

Volume Susceptibility

21

ZL	Zuiderzee Bed
AL	Almere Bed
FL	Flevomeer Bed
LW	Wormer Member
LV	Velsen Bed
HL	Hollandveen Member
LWi	Wierden Member

Sand, coarse
Sand, medium
Sand, very fine
Clay
Peat
Shells

Figure 10: Lithostratigraphic logs of the different cores with susceptibility measurements plotted alongside. The Wormer Member and Velsen Bed are highlighted in black.

3.2 Thermomagnetic analysis

Based on the susceptibility measurements and IRM data, a collection of samples was selected for thermomagnetic analyses. These samples are an attempt to identify every different trend visible in the different susceptibility records. Of VC15 samples 145, 205, 333, 354, 405 and 454 were selected (figure 11). Of core VC17 fewer samples were selected, as the susceptibility trends indicated a weak magnetic signal here. Samples 459, 719, and 874 were selected (figure 12). Of core VC26, again a core with more intensity results, samples 30, 154, 264, 424, and 677 were selected (figure 13).

A typical Curie run, or thermomagnetic analysis, of a greigite sample shows a decrease between 200-420 °C due to the breakdown of greigite to a less magnetic material resulting an irreversible trend of decreased magnetism, (Chang et al., 2014; Dekkers et al., 2000; Roberts et al., 2011a, 2011b; Vasiliev et al., 2008). This trend is a clear distinction between greigite and stoichiometric magnetite. Greigite breaks down before its Curie temperature can be reached. The Curie temperature of greigite is thus unknown. Following the downwards trend, magnetization increases, and a small maximum is reached, as a consequence of the oxidation of iron sulfides into a new mineral. Usually, this is the transition of pyrite into magnetite (Passier et al., 2001). The extent of this new maximum varies depending on the concentrations of pyrite and greigite in the sample. This maximum is gone at 580 °C, the Curie temperature of magnetite. The Néel point of hematite is at ~675 °C. The final run is cooling from 700 °C to room temperature where the Curie point of magnetite does not reappear, which is interpreted as that the previously formed magnetite is oxidized into hematite (Passier et al., 2001).

The different thermomagnetic runs show a variety of curves, as could be expected considering the different lithologies. Samples originating from a lower susceptibility part of the core, often have a low magnetization in the thermomagnetic runs too. The upper part of core VC15 (sample 145) (Fig. 11 A) has a low susceptibility. A sample from this part gives a diamagnetic signal. Considering the presence of shells and thus calcite in the lithology this is

not unexpected. The quartz-glass sample holder itself is also diamagnetic and could potentially too be the cause of the signal. Samples 205 and 333 (Fig. 11 B, C) show a declining trend between 200-400 °C, and the transition of pyrite into magnetite, peaking at about 500 °C, and eventually, oxidizes to hematite. The samples 354, 405, and 454 (Fig. 11 D, E, F) all show the characteristic decrease in magnetism of greigite between 200 – 400 °C. The present magnetite converts quickly to hematite, leaving only a minor maximum at 500 °C.

Core VC17 shows a diamagnetic signal at sample 459 (Fig. 12 A). Considering this core has low susceptibility measurements too, this is likely the quartz diamagnetic signal of the quartz holder. Samples 719 and 874 (Fig. 12 B, C) have a decreasing trend of magnetism with a minimum between 300-400 degrees °C. The subsequent maximum at 500 °C indicates a presence of pyrite being oxidized into magnetite at the higher temperature runs (Fig. 12 B, C). Samples 719 and 874 (Fig. 12 B, C) show the transition into hematite too after the cooling of the final run.

Core VC26 (Fig. 13) has the characteristic pyrite oxidation maximum at about 500 °C in all samples except for sample 667 (Fig. 13 E), which is diamagnetic. The magnetic signal of sample 677 is possibly an artifact of the holder. A clear presence of greigite can be seen in samples 154 and 424 (Fig. 13 B, D). Based upon the decline between 200-400 °C. Sample 264 (Fig. 13 C) contains a small amount of greigite too. The oxidation of the formed magnetite to hematite is also visible in samples 30, 154, 264, and 424 (Fig. 13 A, B, C, D), as in the final run there is no restoration of magnetization level.
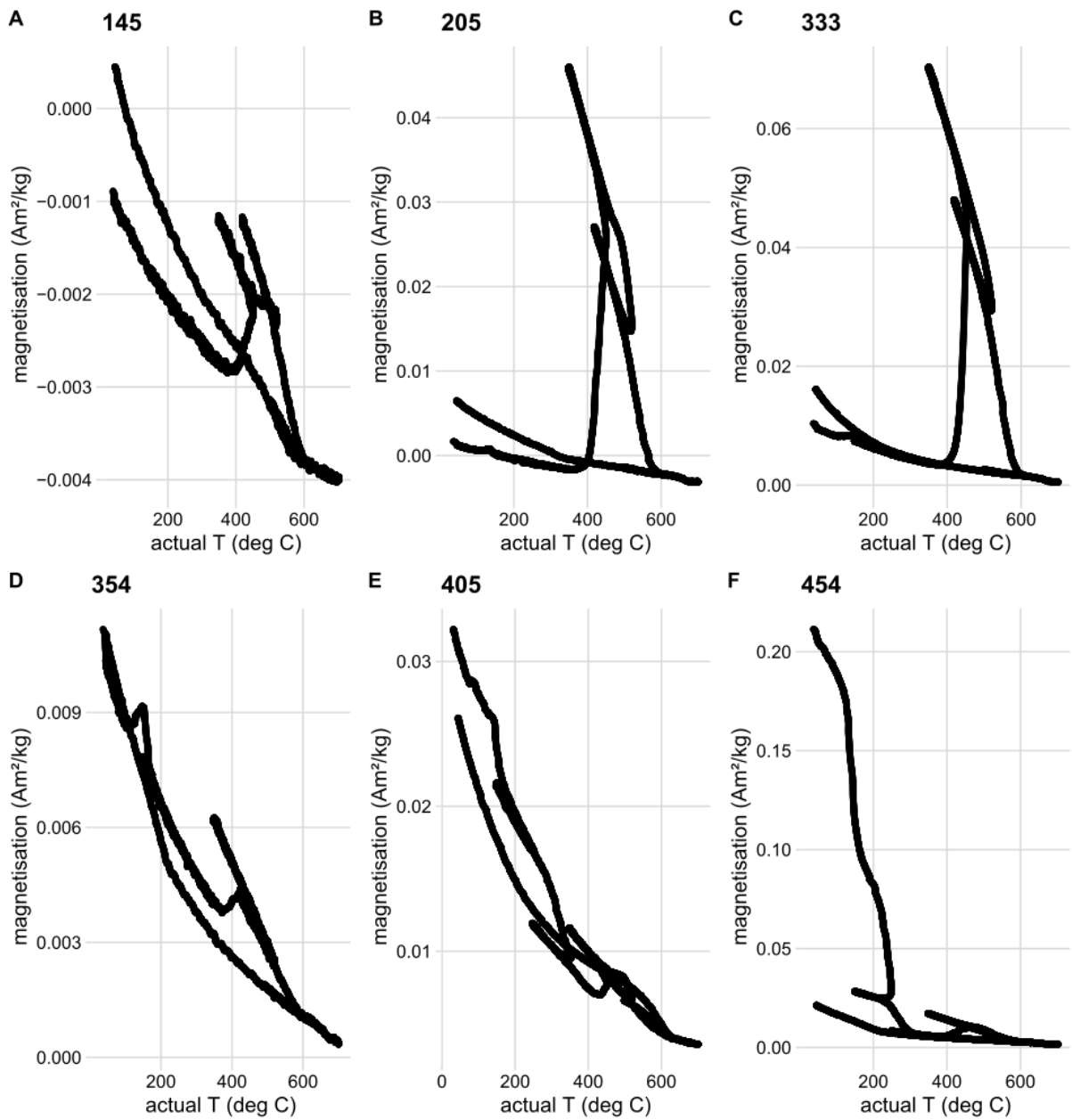
Figure 11: High temperature thermomagnetic runs of core VC15
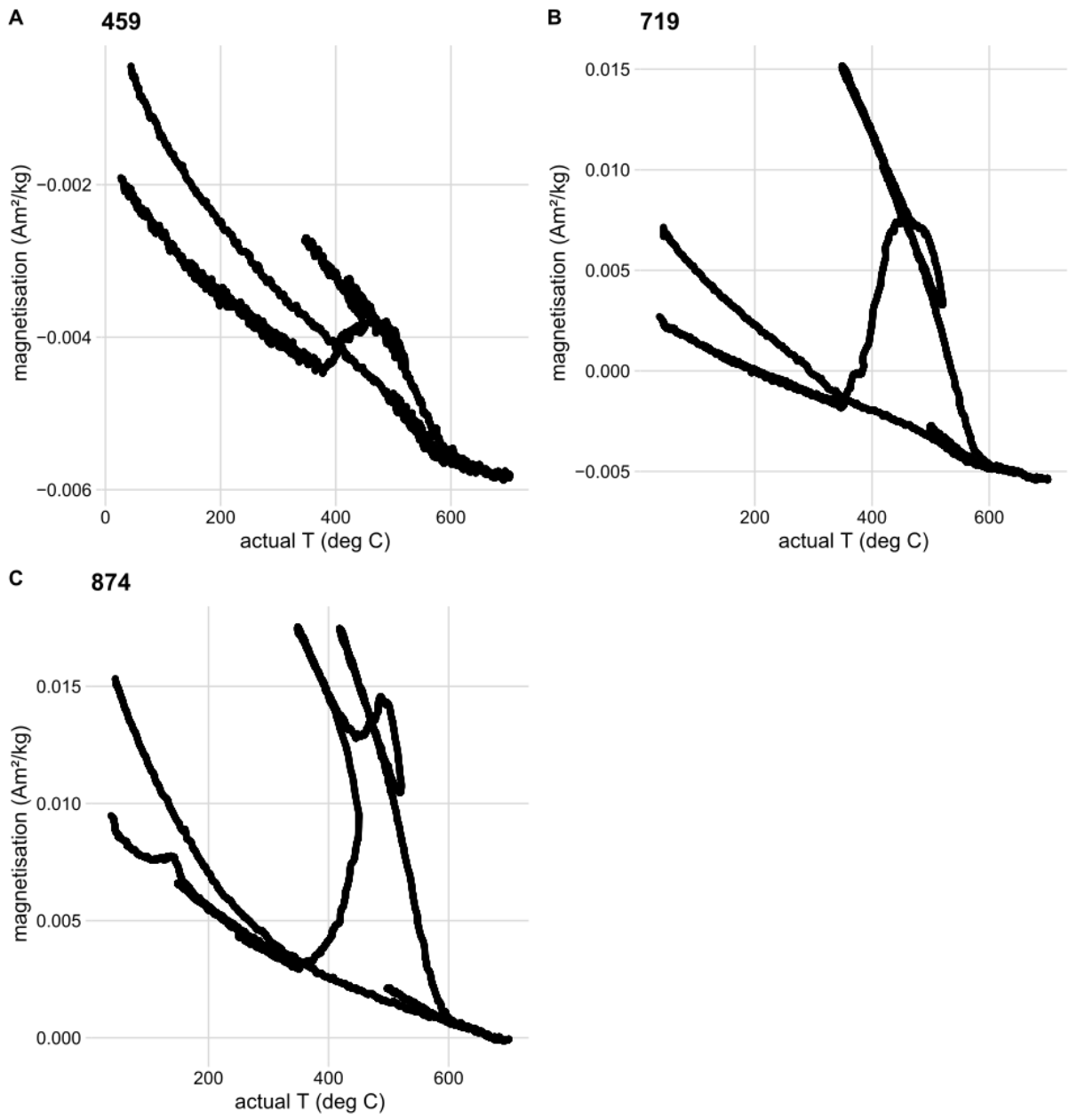
Figure 12: High thermomagnetic runs of core VC17
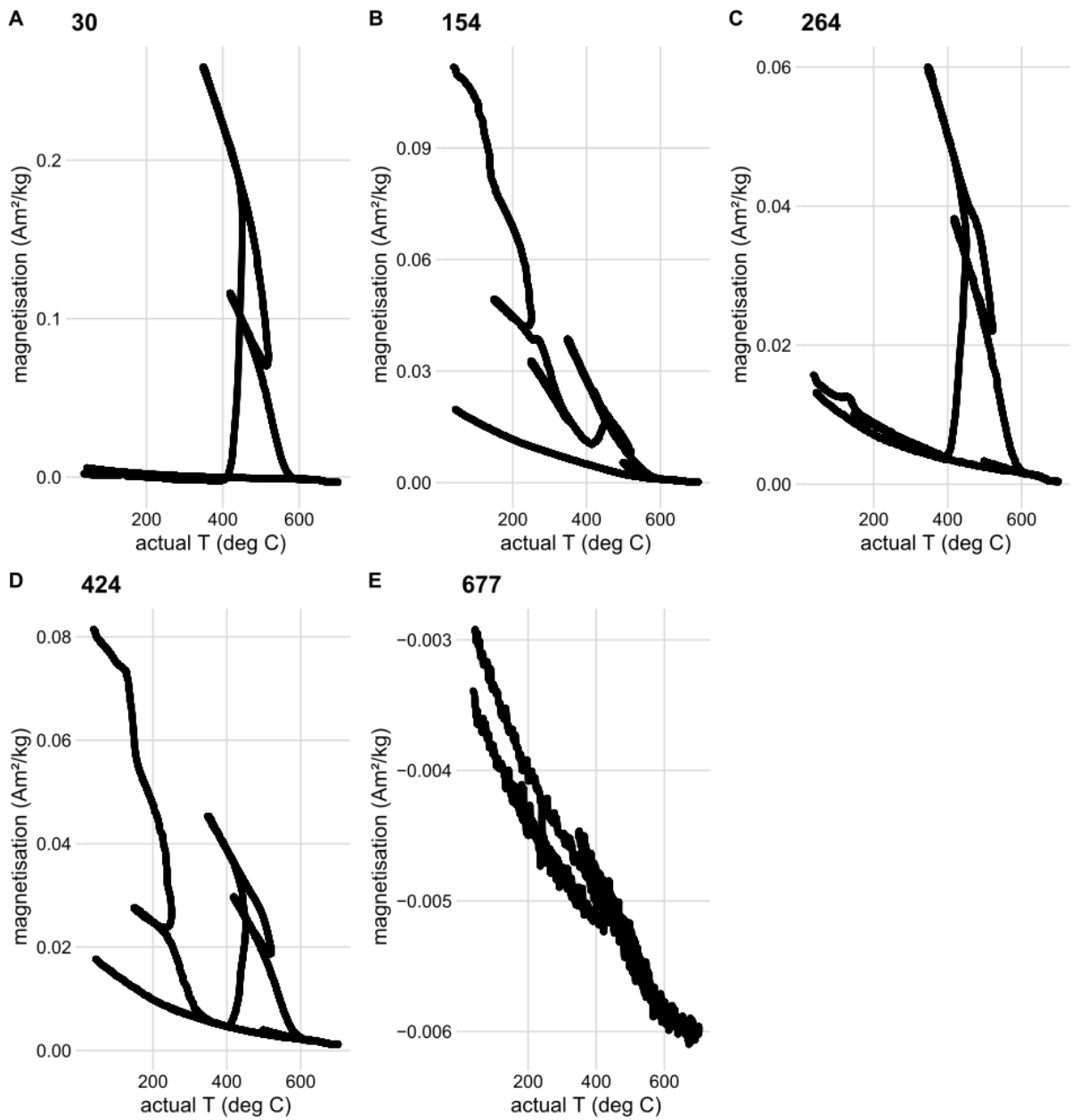
Figure 13: High thermomagnetic runs of core VC26

3.3 Isothermal Remanent Magnetization

Using the Kruiver et al. (2001) workbook, IRM acquisition curves could be fitted consisting of three components. An example of the fits is plotted in figure 14. The first component is interpreted as an artifact of the thermally activated second component and is thus added in the results to the second. SIRM trends correlate to susceptibility and thereby lithology. Most peaks are in the clay sediments of the Wormer Member and Velsen Bed. In table 2, an overview per stratigraphic unit is given. Figure 15 shows the SIRM and $B_{1/2}$ trends of the different cores. VC15 has an average contribution of 97.2% and C1+C2 SIRM of $3.04*10^{-4}$ Am^2 in the Wormer Member (333-347 cm) and a contribution of 97.2% with a SIRM of $9.54*10^5$ Am^2 in the Velsen Bed (354-505 cm). VC26 has an average contribution of 97.5% and a C1+C2 SIRM $4.25*10^7$ Am^2 in the Wormer Member (134-394 cm) and a contribution of 95.5% and a SIRM of $6.04*10^7$ Am^2 in the Velsen Bed (404-647 cm). In comparison, the C1+C2 SIRM of VC17 in the Velsen Bed is $2.16*10^{10}$ Am^2 (874 cm), with a contribution of 95.6 %. The IRM results of the different cores add to the trends found in the susceptibility record (Fig. 10). The component $B_{1/2}$ values of component C2 in the different cores (Fig. 15 C, F, I) show a different and highly variable trend for all three cores. However, for core VC15 and VC26, it is visible that when the SIRM components trends peak, the $B_{1/2}$ shows a regressing trend. High SIRM values coincide with low $B_{1/2}$ values.

   The SIRM of the second component varies between 10^{-6} to 10^{-2} Am^2. A general consistency is visible in all second component $B_{1/2}$ values of the subset, ranging from 52.48 mT to 74.13 mT. Second component DP values show little spread too, ranging from 0.2 mT to 0.34 mT (log units). The contribution of the first two components is about 89% to 100%, and thus quite high. Third component trends show higher variation. SIRM values here range from 10^{-7} Am^2 to 10^{-4} Am^2. $B_{1/2}$ varies between 316.23 to 616.60 mT. DP varies between 0.1 mT to 0.5 mT. The contribution of the third component varies between 0% to 14.1%.

IRM COMPONENT ANALYSIS   VC26 424

component	contribution	SIRM	$\log(B_{1/2})$	$B_{1/2}$	DP
	%	Am^2	mT	mT	mT
1	6,2	1,00E+07	1,22	16,6	0,15
2	92,6	1,50E+08	1,75	56,2	0,25
3	1,2	1,90E+06	2,67	467,7	0,15
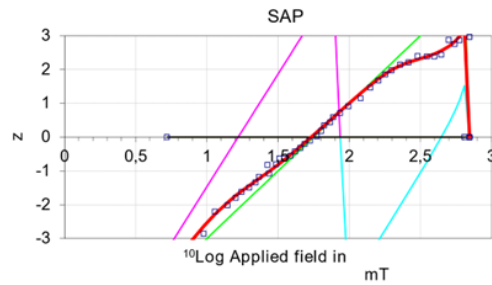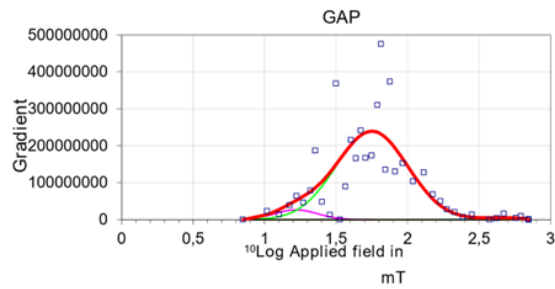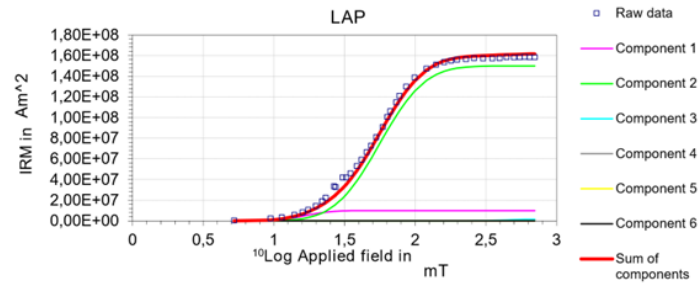
IRM COMPONENT ANALYSIS   VC15 165 cm

component	contribution	SIRM	$\log(B_{1/2})$	$B_{1/2}$	DP
	%	Am^2	mT	mT	mT
1	13,9	3,50E+05	1,40	25,1	0,25
2	79,7	2,00E+06	1,87	74,1	0,25
3	6,4	1,60E+05	2,60	398,1	0,30
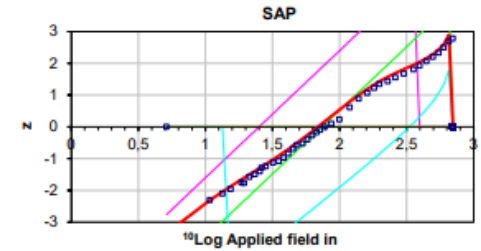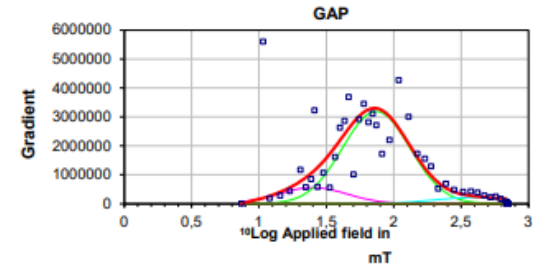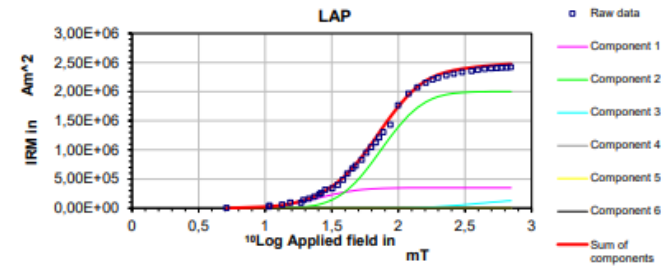
Figure 14: Example of high SIRM IRM acquisition curves of sample 424 from core VC26, and low SIRM IRM acquisition curves of sample 165 from core VC15.

The C1+C2 SIRM mirrors the susceptibility trends of the cores VC15 and VC26 (Fig. 13 A, G) An exception to this is the VC17 core, which shows a different trend for both susceptibility and SIRM C1+C2 (Fig. 15 D). The third component SIRM of VC15, VC17, and VC26 (Fig. 15 B, E, H), mirrors the trends of the C1+C2 components, albeit of different intensity.
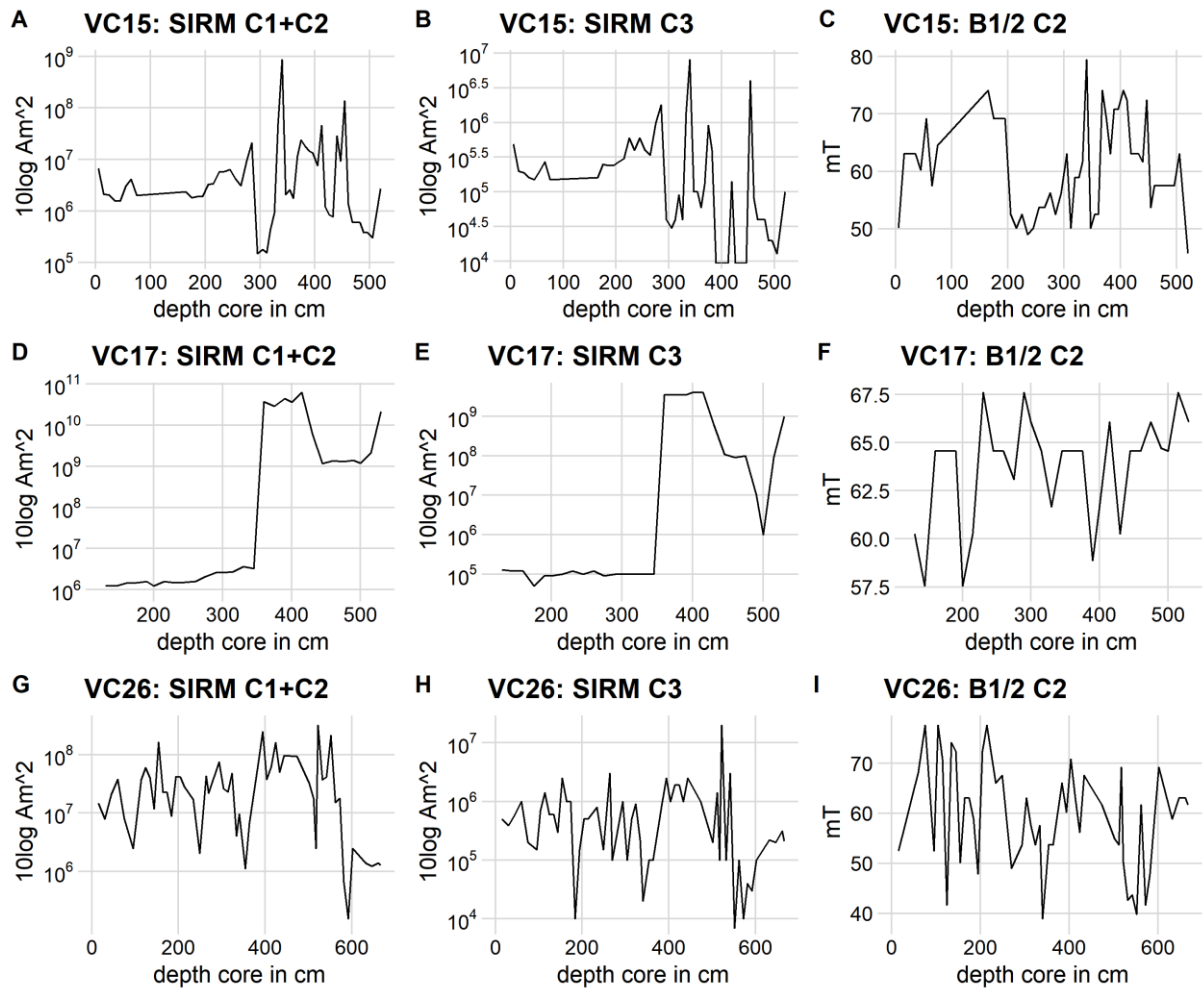
Figure 15: IRM results: SIRM and $B_{1/2}$ of the different components of the different cores.

Table 3 offers a transect of IRM values correlating to selected samples representing the different high/low susceptibility trends of the cores, as indicated by the susceptibility values in the last column. These values largely overlap or are comparable to the samples selected for thermomagnetic analyses. Highlighted in grey are the samples found in the Velsen Bed and the Wormer Member.

Of these samples in the Velsen Bed and Wormer member IRM values $B_{1/2}$ range from 50.12 - 74.13 mT for the first two components, with a DP fluctuating between 0.20 – 0.34 mT. The third component has a $B_{1/2}$ ranging from 300 - 600 mT. And a DP between 0.1 - 0.5 log mT. The SIRM values of the first two components have a magnitude between 10^{-8} - 10^{-4} Am^2. The SIRM values of the third component are of a magnitude 10^{-7} – 10^{-3} Am^2. Generally, the SIRM values are quite high for these samples indicating magnetic interaction.

Using these values most samples fall into the categories of potentially being greigite, or magnetite. Room temperature coercive properties are similar for these minerals, meaning that using solely these magnetic criterions no distinction can be made (Da Silva et al., 2012; Liu et al., 2017; Peters & Thompson, 1998; Vasiliev et al., 2007). A preliminary distinction can be made however for the third component of samples VC26: 264 & 424 (Table 3, red script). These have a DP of 0.1 and 0.15 mT. Which indicates magnetite or greigite of a biological origin (Egli, 2004; Kruiver & Passier, 2001).

	Depth from top core	C1+C2 contribution	C1	C2	C1+C2 SIRM			C3			
	cm	%	SIRM pAm²	SIRM (pAm²)	SIRM pAm²	LOG(B$_{1/2}$)	DP	%	SIRM (pAM²)	LOG(B$_{1/2}$)	DP
Zuiderzee Bed											
VC15	5-75	92.37	2.07E+05	1.77E+10	2.91E+06	1.84	0.25	12.54	2.96E+09	2.64	0.49
VC26	15	96.72	2.50E+05	1.45E+07	1.48E+07	1.72	0.25	3.28	5.00E+05	2.57	0.30
Almere Bed											
VC15	165 -195	89.70	2.50E+05	1.74E+06	1.99E+06	1.85	0.28	10.25	2.23E+05	2.60	0.45
VC17	474	90.47	1.34E+05	1.10E+06	1.23E+06	1.78	0.25	9.53	1.30E+05	2.55	0.35
VC26	30	95.35	4.50E+05	7.55E+06	8.00E+06	1.76	0.24	4.65	3.90E+05	2.79	0.30
Flevomeer Bed											
VC15	205-295	90.25	6.92E+05	5.53E+06	6.23E+06	1.72	0.25	9.76	2.49E+06	2.41	0.47
VC17	489 -759	93.89	8.63E+08	9.50E+09	1.04E+10	1.80	0.26	6.11	9.25E+08	2.65	0.29
Hollandveen Member											
VC15	305-326	85.93	6.45E+04	3.55E+05	4.20E+05	1.76	0.33	14.08	5.00E+04	2.63	0.40
VC17	744-859	94.24	5.69E+08	1.20E+10	1.25E+10	1.81	0.29	5.76	1.00E+09	2.72	0.22
VC26	95-124	95.46	2.08E+06	2.49E+07	2.70E+07	1.77	0.21	4.54	7.13E+05	2.47	0.27
Wormer Member											
VC15	333-347	97.23	1.27E+07	2.91E+08	3.04E+08	1.80	0.23	2.73	3.17E+06	2.73	0.30
VC26	134-394	97.46	2.22E+06	4.02E+07	4.25E+07	1.77	0.25	2.54	7.37E+05	2.63	0.18
Velsen Bed											
VC15	354-505	97.22	9.54E+05	1.06E+07	1.16E+07	1.79	0.24	2.78	3.18E+05	2.57	0.22
VC17	874	95.58	2.00E+09	1.96E+10	2.16E+10	1.82	0.28	4.42	1.00E+09	2.67	0.30
VC26	404-647	95.46	3.17E+06	5.72E+07	6.04E+07	1.75	0.25	4.54	1.74E+06	2.56	0.25
Pleistocene											
VC15	520	96.50	1.55E+05	2.60E+06	2.76E+06	1.66	0.30	3.50	1.00E+05	2.79	0.30
VC26	667	85.91	8.00E+04	1.20E+06	1.28E+06	1.79	0.34	14.09	2.10E+05	2.57	0.30

Table 2: Average IRM values of the different cores combined per stratigraphic unit.

Depth core (cm)	C1+C2 contribution %	C1 SIRM pAm^2	C2 SIRM (pAM^2)	C1+C2 SIRM pAm^2	LOG(B1/2)	B1/2 mT	DP	C3 %	SIRM (pAM^2)	LOG(B1/2)	B1/2 mT	DP	Susceptibility Volume Units
VC15													
165	93.6	3.50E+05	2.00E+06	2.35E+06	1.87	74.13	0.25	6.4	1.60E+05	2.6	398.11	0.3	0.02
205	92.4	3.00E+05	3.00E+06	3.30E+06	1.72	52.48	0.3	7.6	2.70E+05	2.5	316.23	0.5	0.03
333	97.2	8.00E+06	4.10E+07	4.90E+07	1.79	61.66	0.2	2.8	1.40E+06	2.6	398.11	0.5	0.26
354	91.8	7.00E+04	1.05E+06	1.12E+06	1.73	53.70	0.32	8.2	1.00E+05	2.67	467.74	0.3	3.69
405	100	3.35E+05	7.35E+06	7.69E+06	1.87	74.13	0.2	0	0.00E+00	0	1.00	0	0.28
454	97.2	5.00E+06	1.32E+08	1.37E+08	1.73	53.70	0.22	2.8	4.00E+06	2.79	616.60	0.3	0.67
VC17													
135	90.5	1.34E+05	1.10E+06	1.23E+06	1.78	60.26	0.25	9.5	1.30E+05	2.55	354.81	0.35	0.02
380	89	4.41E+09	2.40E+10	2.84E+10	1.81	64.57	0.23	11	3.50E+09	2.6	398.11	0.3	0.05
535	95.6	2.00E+09	1.96E+10	2.16E+10	1.82	66.07	0.28	4.4	1.00E+09	2.67	467.74	0.3	0.06
VC26													
30	95.4	4.50E+05	7.55E+06	8.00E+06	1.76	57.54	0.24	4.6	3.90E+05	2.79	616.60	0.3	0.04
154	98.5	3.00E+06	1.60E+08	1.63E+08	1.7	50.12	0.25	1.5	2.50E+06	2.67	467.74	0.3	2.65
264	93.5	1.85E+06	4.10E+07	4.29E+07	1.73	53.70	0.28	6.5	3.00E+06	2.75	562.34	0.1	0.23
424	98.8	1.00E+07	1.50E+08	1.60E+08	1.75	56.23	0.25	1.2	1.90E+06	2.67	467.74	0.15	1.34
667	85.9	8.00E+04	1.20E+06	1.28E+06	1.79	61.66	0.34	14.1	2.10E+05	2.57	371.54	0.3	-0.01

Table 3: IRM data of selected samples correlating to the different susceptibility trends of the cores. Highlighted in grey are the samples originating from the Velsen Bed and Wormer Member. Red are values indicating a potential biological origin of the magnetic mineral.

Further information about the magnetic grain size can be gained via the ARM/IRM ratio. A high ratio value means a finer grain size, while low ratio values indicate a coarsening of the magnetic grains (Rowan et al., 2009). The three different cores have comparatively low values, indicating coarse grains and some peaks indicating fine grains. These can be found in the Hollandveen member for VC15 and VC17 (Fig.16 A, B), the Velsen Bed for VC26 (Fig. 16 C).
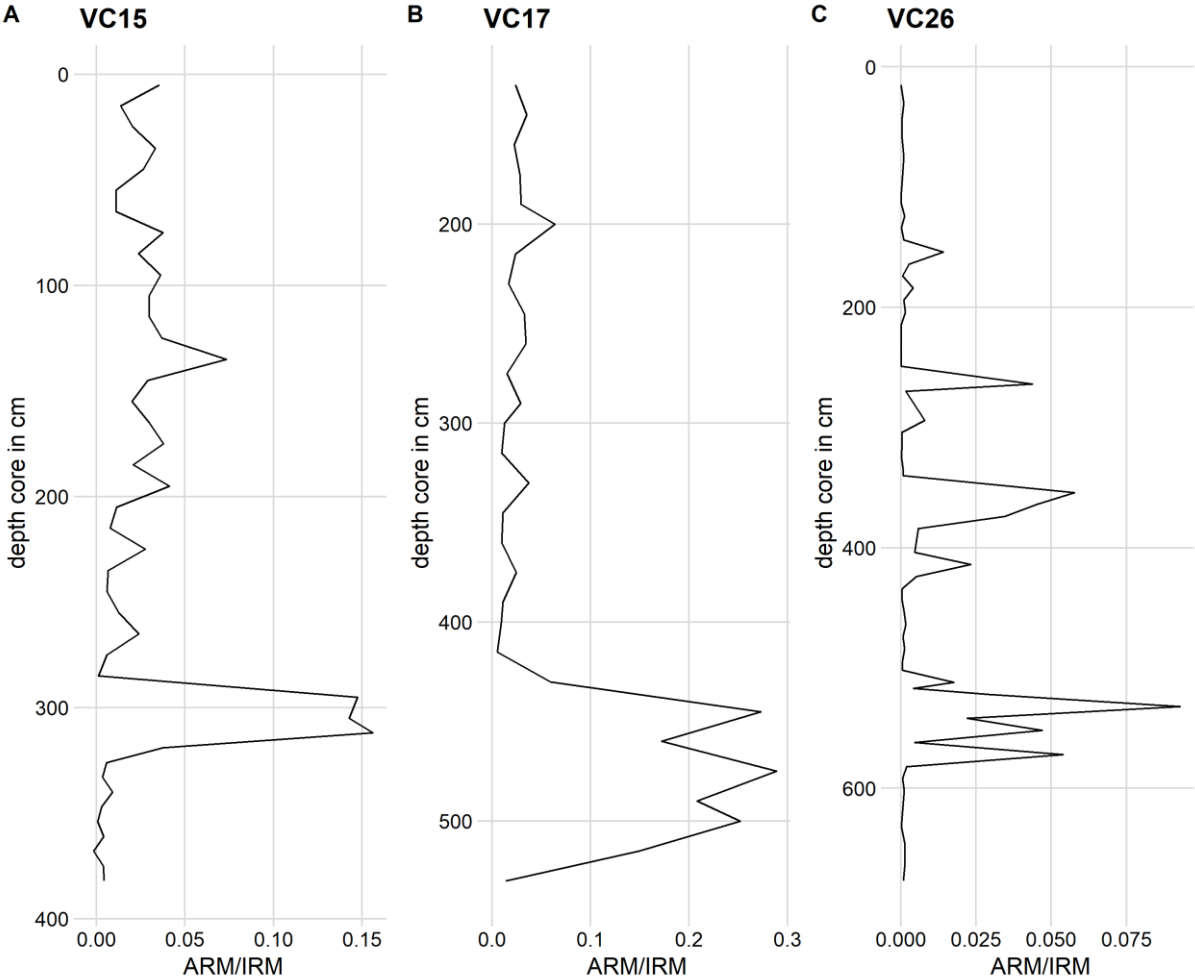
Figure 14: ARM/IRM-ratio of the three different cores

3.4 Paleomagnetic directions

Declination	Inclination	Intensity	MAD
73.29	70.02	5195.98	1.18

Declination	Inclination	Intensity	MAD
86.53	48.33	6149.08	0.68

Figure 15: Zijderveld diagrams of different samples of different types of NRM sample quality. Sample 404 is of quality type 1, sample 562 of quality type 2, sample 677 of quality type 3.

	VC15	VC17	VC26	Total	%
Number of Samples	52	38	58	148	100
Type 1	19	2	26	47	31.76
Type 2	15	9	28	52	35.14
Type 3	18	27	4	49	33.11

Table 4: The number of samples belonging to the different NRM quality and the size of the respective group.

Paleomagnetic directions were interpreted via Zijderveld diagrams. Figure 17 gives an example of samples of different quality and the interpretation made. The samples were demagnetized in small field steps. When filtering out the smallest and highest field steps a directional component becomes clear. Between the different samples generally the higher field steps yielded an interpretable directional component. The samples were separated in three types of different quality (Table 4). Type 1 with a magnetic component through the origin and a MAD angle $< 5°$, type 2 with a magnetic direction not through the origin or a MAD angle $> 5°$, and type 3, a sample of which no magnetic vector could be determined. Table 4 shows the number of samples belonging to each type. Combining the samples of all cores gives a quite equal distribution of the samples over the types.

In figure 18 the inclination and (relative) declination records are shown of the cores VC15 and VC26; core segment separations are indicated by the blue lines. Results of core VC17 are omitted since the number of meaningful data points is too low. Samples of quality type 1 or 2 are primarily found in the clay rich layers identified as the Velsen Bed or Wormer Member. Other lithologies and especially the more sandy ones result in less robust data points, as is visible in core VC15 (Fig. 18 A, C) by the lack of data points in the top and bottom parts of the core. Inclinations in core VC15 (Fig. 18 A) and VC26 (Fig. 18 B) fluctuate around 60-70°, albeit that core VC15 shows lower values tha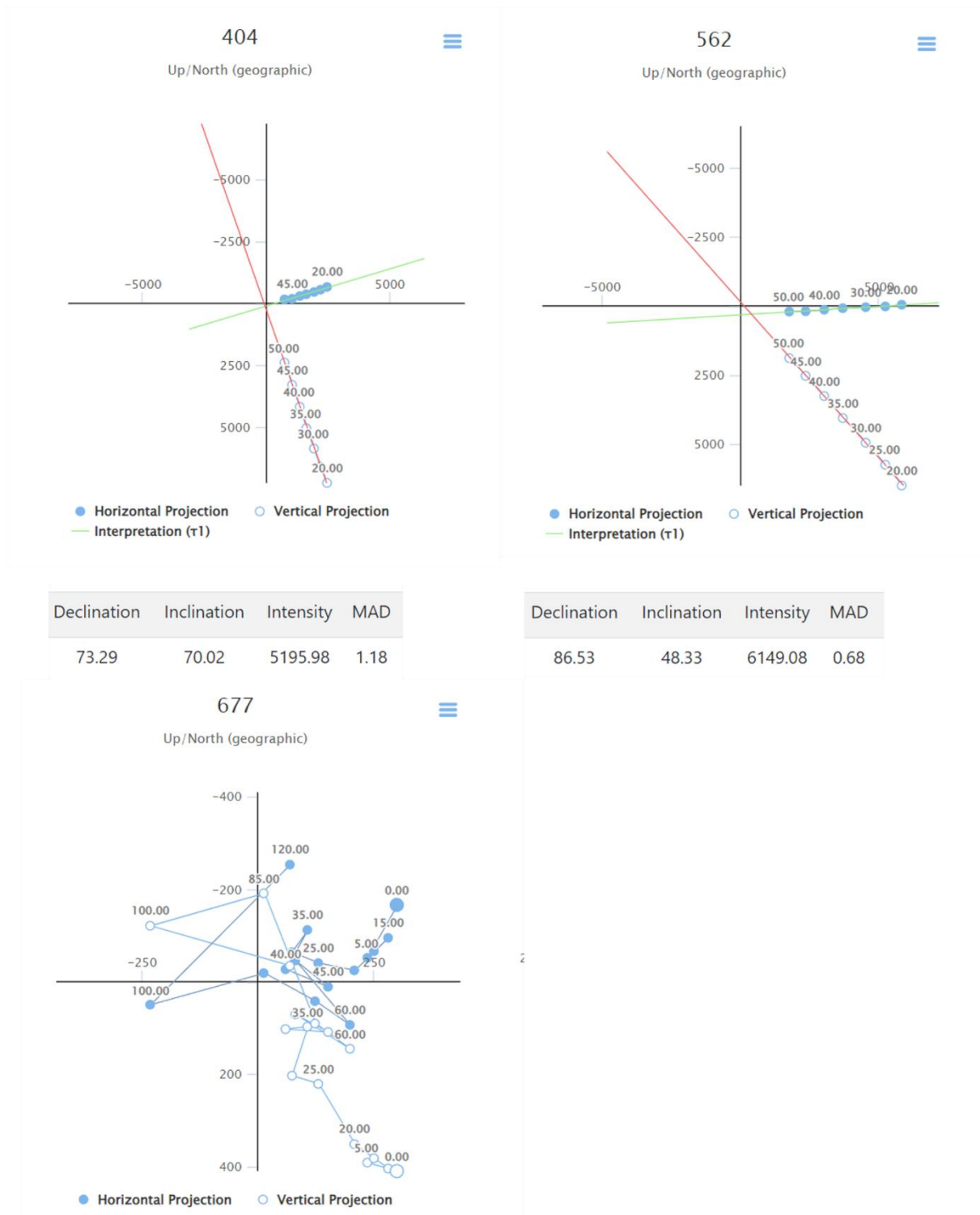n VC26. The declination of VC15 (Fig. 18 C) fluctuates between values lying apart more than 100°, while the declination values of VC26 (Fig. 18 D) vary with about 80°.

Notable was the amount of gyroremanent magnetization (GRM) in the samples. A GRM is a magnetic component obtained by rotating an anisotropic magnetic mineral prone to acquire GRM, while under the influence of an alternating magnetic field (Stephenson, 1993; Snowball, 1997). This is also a strong indication of the presence of greigite, although biologically formed greigite does not necessarily show GRM (Roberts et al., 2011). Diagenetically formed greigite frequently contains closely packed greigite crystals, creating a bias field and enabling GRM acquisition (Chang et al., 2014). Core VC26 show signs of GRM in all interpretable samples, although the intensity in which GRM is found differs. In core VC17 every interpretable sample shows signs of GRM too. Core VC15 differs, as here a distinction is visible. From sample 433 and downwards GRM is visible, while interpretable samples higher in the core do not showcase signs of GRM.
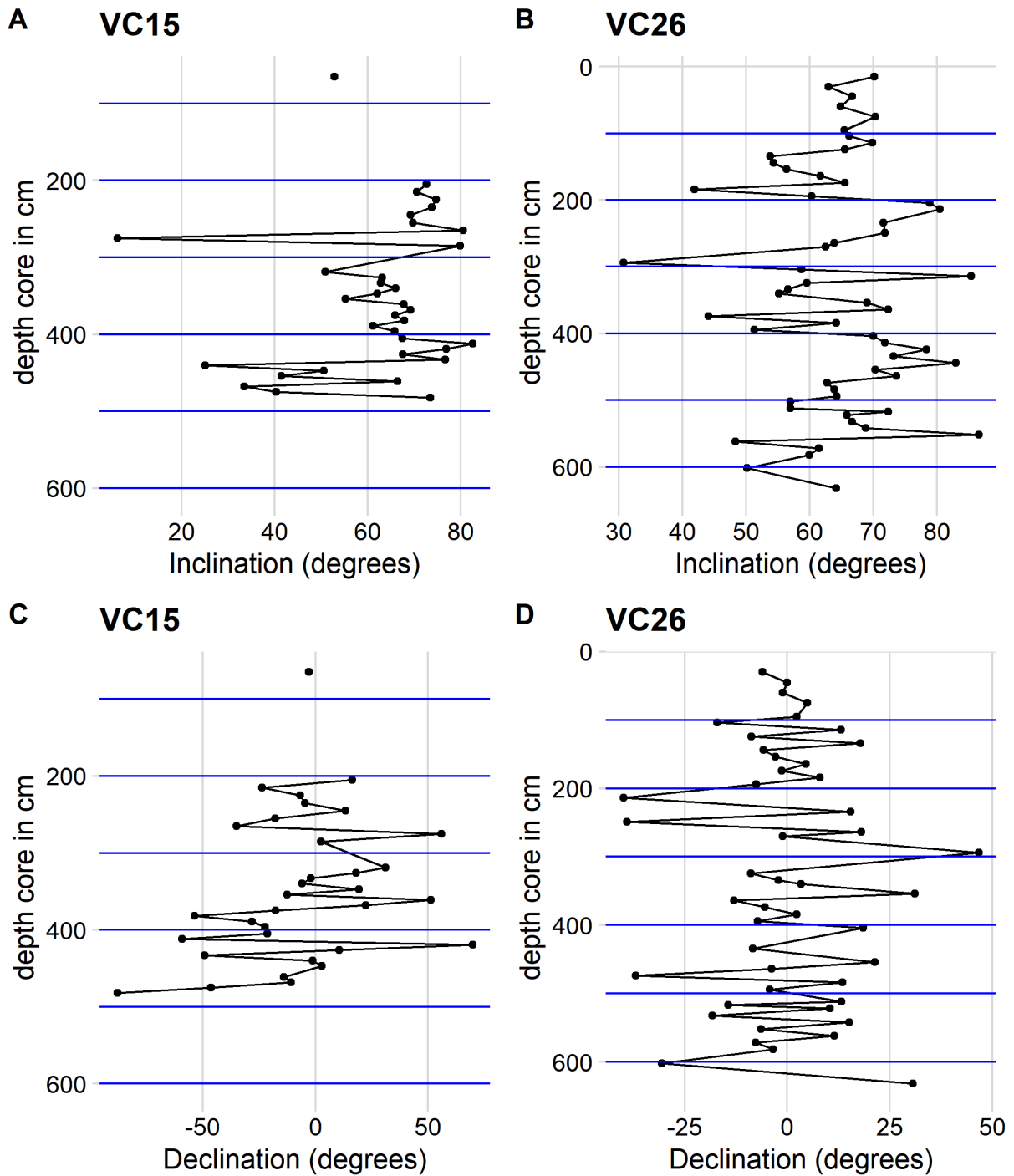
Figure 18: Inclination and (relative) declination records of VC15 and VC26. VC17 was omitted due to a low number of meaningful datapoints. Considering the gap in data between the first datapoint of VC15 and the subsequent data points, this data point was not connected. The different core segments are indicated by blue lines.

3.5 Relative Paleointensity
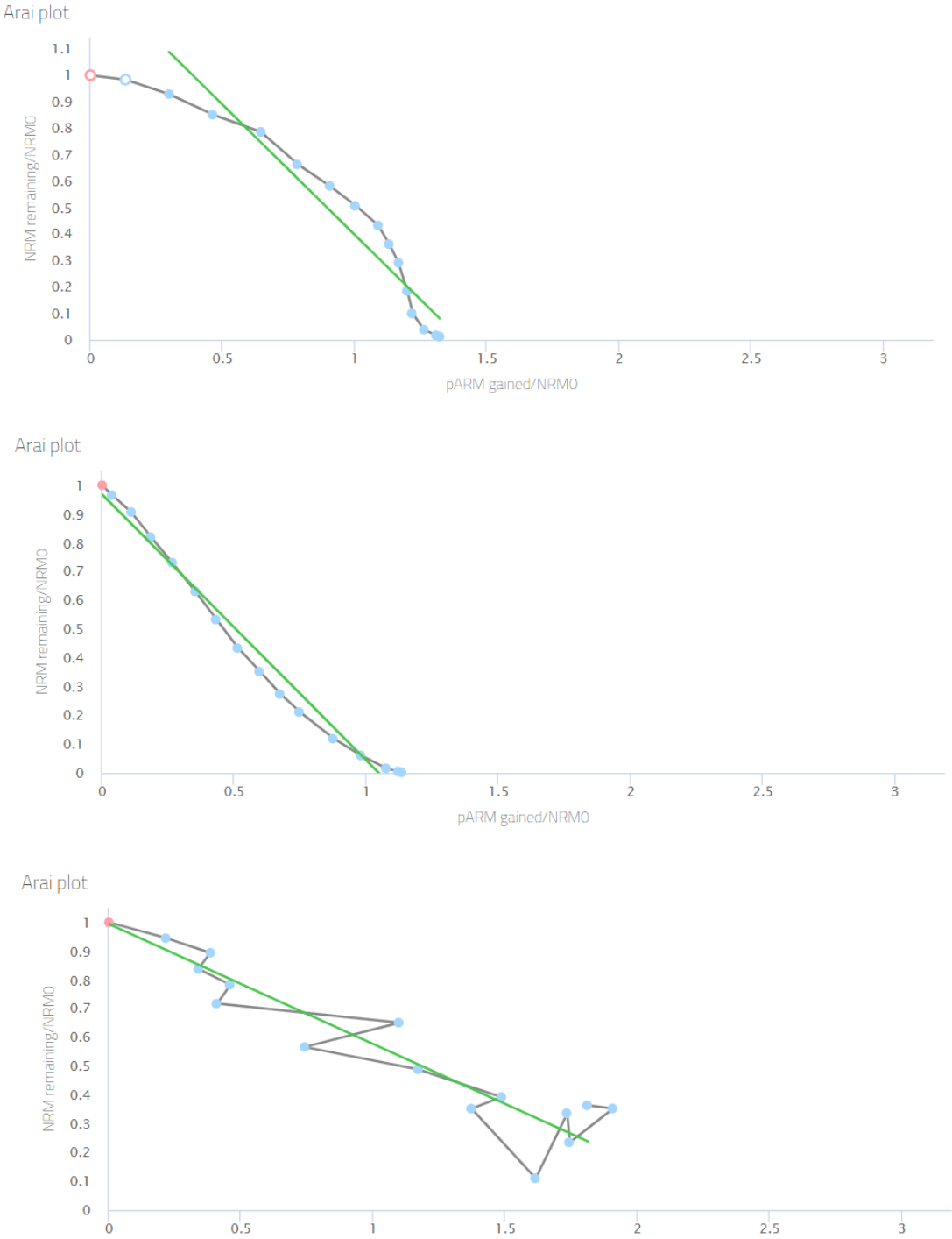
Figure 19: Arai diagrams of three different samples of which the relative paleointensity slope (green line) is calculated from selected points
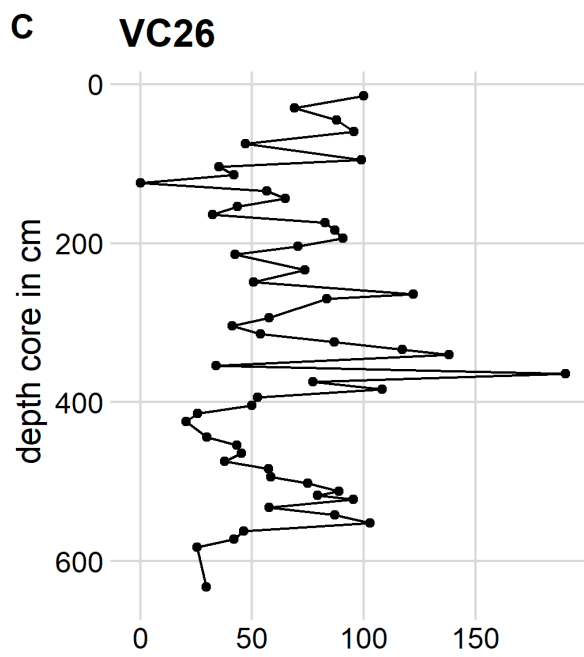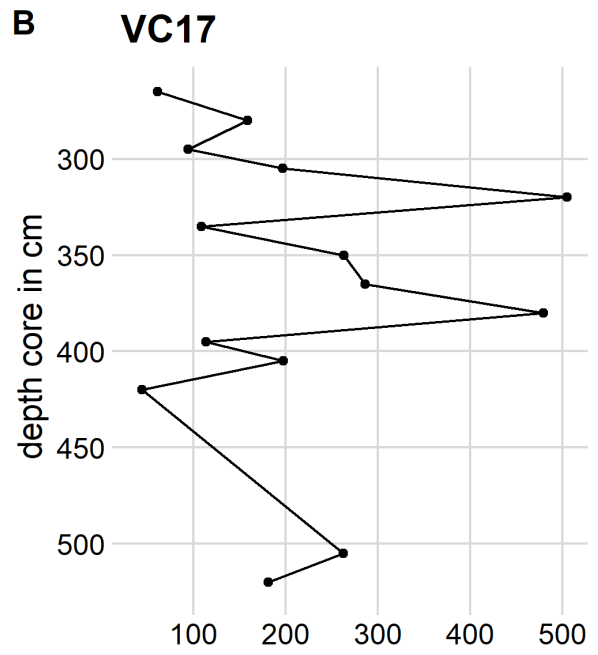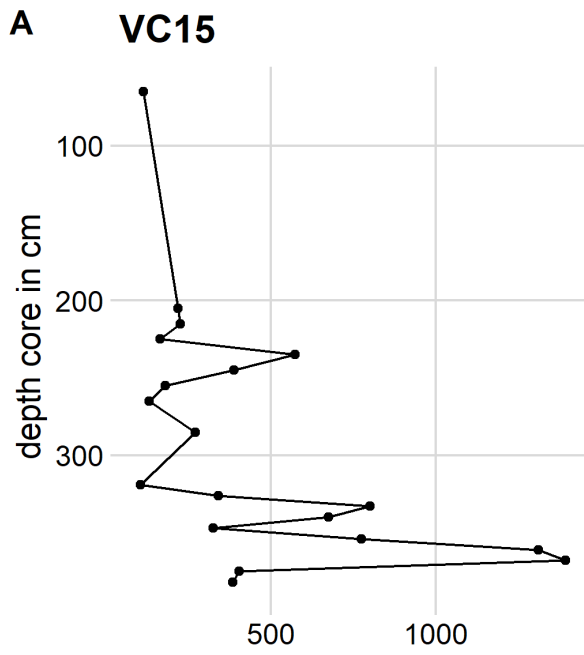
Figure 20: The relative paleointensity slopes of the different cores

RPI	VC15	VC17	VC26
Total amount of samples	52	38	58
Pseudo-Thellier possible	19	14	53
%	36,5	36,8	91,4

Table 5: The total number of samples per core and the amount on which pseudo-Thellier could be performed.

A relative paleointensity slope record was created (Fig. 20), from the slopes calculated as shown in the Arai diagrams (Fig. 19). Considering that calibration formulas set up lavas do not work for sedimentary samples, a calibrated relative paleointensity record could not be created and so only the slope was calculated. VC26 contains far more data points than VC15 and VC17 indicating a better sample quality. This becomes also apparent from table 5 which shows that a pseudo-Thellier slope could be calculated in ~91% of the samples in core VC26. On 36.5 % of the samples of VC15, and 36.8% of the samples of VC17 (Table 5) Pseudo-Thellier could be performed. The data density is the highest in the Velsen Bed and Wormer Member for all cores. Slope numbers of the different cores vary wildly with VC15 reaching values below three times as high as the highest value of VC17, while VC26 values remain equal to the lowest parts of VC15 and VC17.

3.6 X-Ray Fluorescence Measurements

For cores VC15 and VC26 an Rb/Sr record was created (Fig. 21 B, D). Based on the susceptibility measurements of core VC15, only the high-interest interval of 300 cm and downwards was measured (Fig. 21 A). Since Sr is leached more easily than Rb, the proxy works as an indicator of weathered terrigenous detritus input (e.g. Chen et al., 1999; Liu et al., 2017). The proxy seems to show a comparable pattern, where higher susceptibility measurements match with higher Rb/Sr values (Fig. 21 A, C). However, considering that the proxy is used in a lacustrine/riverine setting instead of a terrestrial/marine environment where it was designed for, the reliability of these results is questionable.
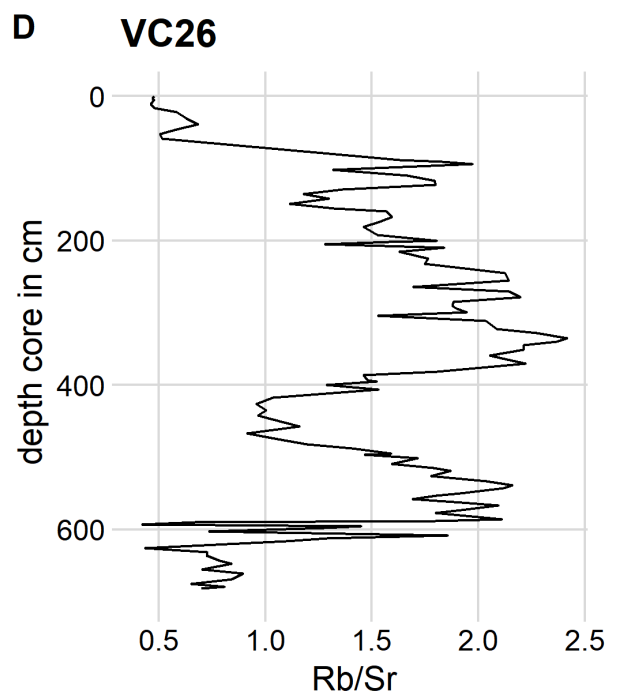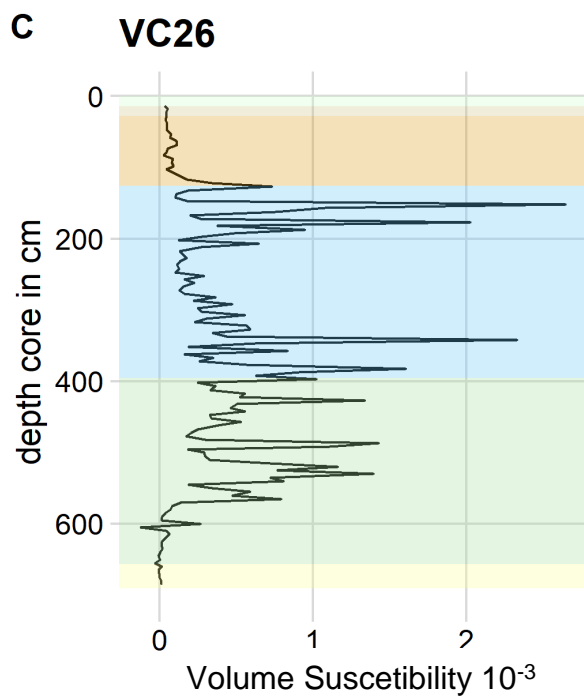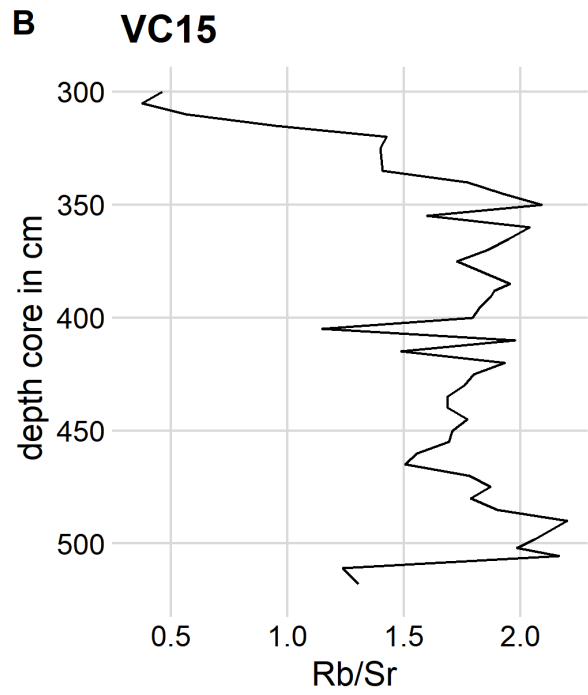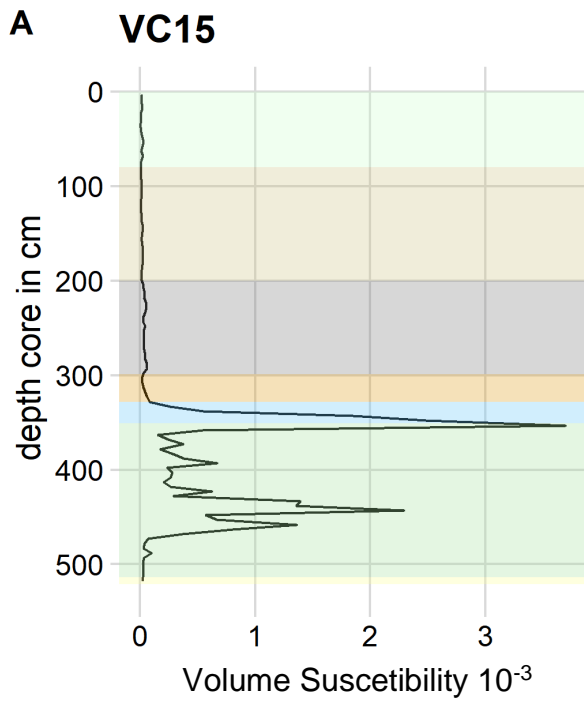
A **VC15**

B **VC15**

C **VC26**

D **VC26**

ZL	Zuiderzee Bed
AL	Almere Bed
FL	Flevomeer Bed
LW	Wormer Member
LV	Velsen Bed
HL	Hollandveen Member
LWI	Wierden Member

Figure 21: Magnetic susceptibility of the three cores against depth measured from the top of the cores and the legend. Different colors indicate the different layers.

4. Discussion

4.1 Magnetic carriers
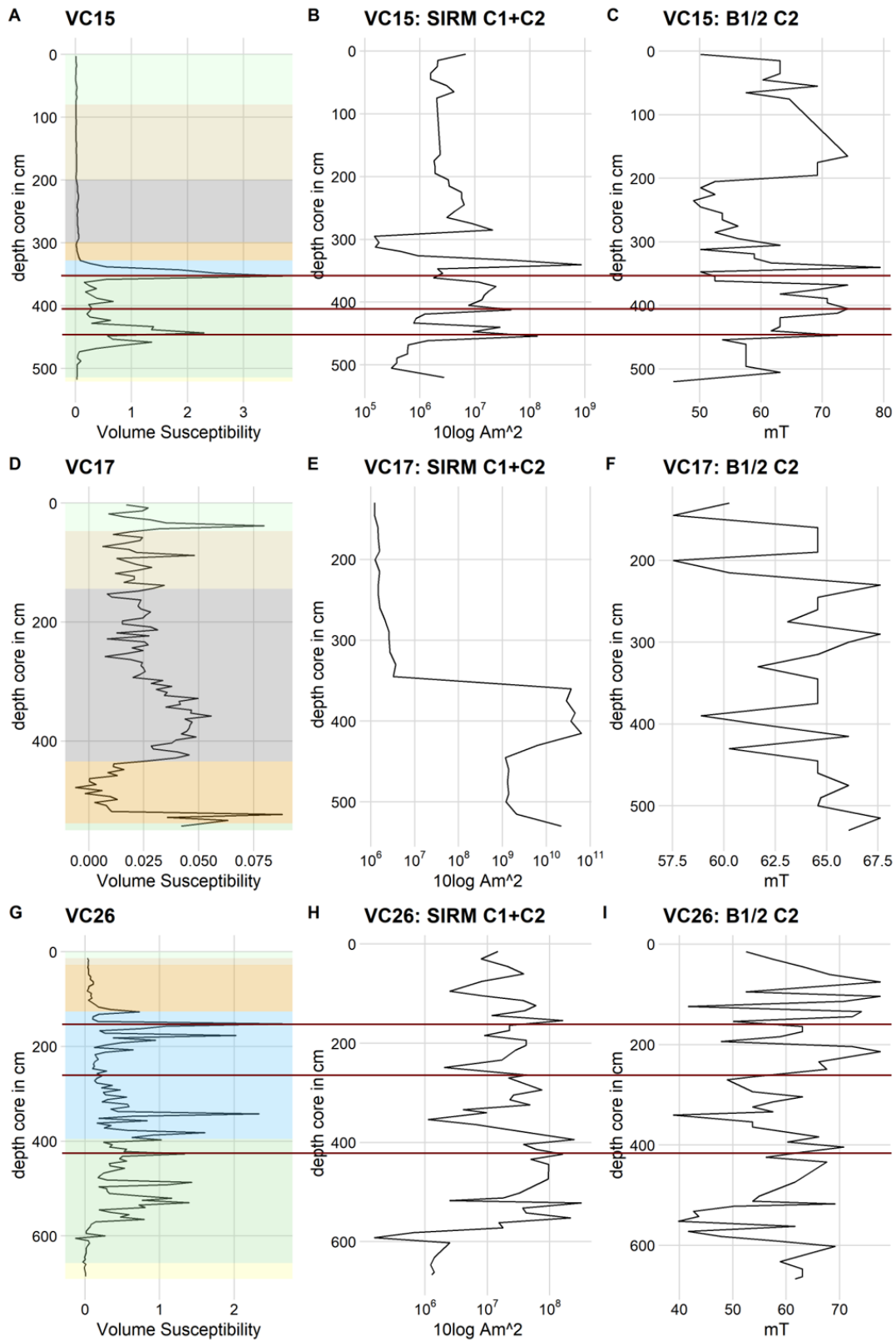
ZL	Zuiderzee Bed
AL	Almere Bed
FL	Flevomeer Bed
LW	Wormer Member
LV	Velsen Bed
HL	Hollandveen Member
LWI	Wierden Member

Figure 22: Magnetic susceptibility and IRM measurements of the three cores against depth measured from the top of the core. Different colors indicate the different layers.

A comparison of the figures of the results shows that there is a clear part of the cores that shows an increase in magnetism (Fig. 22). Susceptibility shows a clear increase in the parts correlating with the Velsen Bed and the Wormer Member. Relative paleointensity and NRM direction results show a larger data density in the same members (Fig. 18 & 20). These stratigraphic members have been highlighted in figure 22, alongside susceptibility, the combined SIRM of component 1 and 2, and the $B_{1/2}$ of the second component for the three cores. The thermomagnetic runs of which was decided that they contain greigite are indicated by red lines in the figure.

As the stratigraphic members are more lithostratigraphic facies than chronostratigraphic, the area and depth at which they occur vary widely. Other sections of the core show a lower susceptibility and smaller data density of the parts outside of the Velsen Bed and the Wormer member. Considering the lack of the Velsen Bed and Wormer Member, it is fitting that no clear signal of greigite was found there.

Looking at the graphs, the combined higher values for susceptibility, SIRM, and $B_{1/2}$ seem indicative of greigite presence. As is illustrated by results of the thermomagnetic runs indicating the presence of greigite in the higher value sections of the VC15 and VC26 cores. VC17 has comparatively low susceptibility values, and thermomagnetic runs were non conclusively indicative of greigite.

The thermomagnetic runs and IRM results show that parts of the different cores, and especially VC15 & VC26 have a strong magnetic signal carried by greigite. A distinction is not easily possible between the different greigite types present. As was stated before, magnetotactic bacteria are capable of producing small magnetite or greigite crystals.

Considering this is common in Quaternary suboxic or anoxic environments (Da Silva et al., 2012; Kirschvink & Chang, 1984; McNeill et al., 1988; Stolz et al., 1986) it is possile that in these samples a form of the biologically formed mineral is also present. The third component of samples VC26: 264 & 424 (Table 3, red script) have a DP of 0.1 and 0.15, could be interpreted as indicative of a magnetotactic origin of the carrier (Egli, 2004a, 2004b; Kruiver & Passier, 2001; Pósfai et al., 2001). Considering that magnetite magnetosomes dissolve rapidly in sulfate-reducing diagenetic environments (Vasiliev et al., 2008), which are required for greigite to form, it is unlikely that the biologically produced minerals are magnetite, but rather they would be greigite. However, higher $B_{1/2}$ values in the same interval are beyond the range of greigite. Furthermore, the low percentages make it a less robust component to add value. The ARM/IRM ratio of VC26 (Fig. 22 C) shows high values in the Velsen Bed, indicating fine grains. This matches with the idea that magnetotactic bacteria produce fine grained greigite. However, this interpretation has serious flaws, as the jump in values could also indicate the difference between greigite and non-greigite as a zero order interpretation. The primary conclusion is thus that diagenetic greigite was found.

4.2 Greigite formation

As previously mentioned, greigite is an iron sulfide and is formed in sulfate-reducing environments. In these settings, greigite is a precursor to pyrite. Clastic sediments containing iron-bearing minerals (Fe^{2+}) react with the sulfide (HS^-) produced by the bacteria in this environment. In order to prevent pyritization and produce greigite, this reaction has to be halted. Three mechanisms have been distinguished based on case scenarios that do so. Halting factors are: (1) The amount of dissolved sulfate (SO_4^{2-}) (aq) available in the pore waters. (2) The availability of organic matter (OM), as well as how reactive it is to be used by microbiota. (3) The amount of reactive iron which is released from minerals in detritus (Berner, 1984; Roberts et al., 1996; Roberts & Weaver, 2005). The logic behind these mechanisms is that it takes a double amount of elemental sulfur to convert greigite (Fe_3S_4) into pyrite (FeS_2), resulting that when a surplus of Fe^{2+} over HS^- exists, the pyritization process will be halted and greigite, being the intermediate product, will be preserved (Fu et al., 2008; Kao et al., 2004).

Considering the complex history of the Lake IJssel, ranging between riverine, intertidal, lacustrine, and marine, a few case studies shall be discussed, to help clarify the different mechanisms enabling greigite formation. Several authors already mention examples where these mechanisms are at play. In the case of a marine sedimentary environment, there is an abundance of sulfate, to be used by microbes. Blanchet et al., (2009), Chang et al. (2014) and Kao et al. (2004) argue that the availability of OM and thus HS^- released by microbes can be controlled by the concentration of dissolved iron. Iron can enter the cycle in several ways, among which as detrital minerals, or as a coating from which Fe^{2+} dissolves. In case of a Fe^{2+} surplus, the subsequent HS^- deficiency halts the transformation of greigite into pyrite, and the greigite is preserved. Greigite was reported in rapidly deposited marine sediment. Here, organic-poor and terrigenous-rich sedimentary layers allow for the formation of diagenetic greigite. A case like this should have greigite peaks correlating with high Rb/Sr ratios, indicating stronger detrital contribution. The availability of reactive OM is thus the limiting factor in these sections.

Lacustrine environments offer a different availability of resources. Detrital iron-bearing minerals and OM to be used by bacteria are more abundant and characterized by low Rb/Sr ratios. These are logically not the limiting factors. A lack of dissolved sulfide is brought forward by (Roberts et al., 1996) as the cause of greigite preservation. In lake settings dissolved sulfide concentrations are typically low, favoring the preservation of greigite by sulfide consumption over the complete transformation to pyrite.

A clear contrast is illustrated by Chang et al., (2014). In the same Miocene Black Sea section the depositional environment switches from a marine setting to a lacustrine setting. In these specific limnological settings, it was argued that small amounts of dissolved sulfide react with abundant iron, making the dissolved sulfate concentration and biogenic productivity the limiting factors, allowing greigite preservation.

A more complex setting is brought forward by Liu et al. (2017). In the Tisa section in Romania (12.8 Ma – 12.2 Ma), a transition is visible, from fully marine to lacustrine. An open marine sea is connected with a brackish basin via a strait, allowing the influx of fresh water. While in marine waters with high sulfate concentrations, bacterial sulfate reduction is efficient enough to produce abundant HS^-, freshwaters on the contrary have a lower sulfate concentration (Berner, 1984). This mechanism enables the preservation of greigite. A correlation between high ratios of Rb to Sr or Ca to Al, and thus continental input and biogenic production was not found. Terrestrial input and OM were deemed not to be limiting factors. The influx of freshwater and by extension the insufficiently low sulfate concentration was consequently ruled as a limiting factor and reason for greigite preservation.

As mentioned before, the greigite from the Lake IJssel cores is present in the Velsen Bed and Wormer Member. These deposits are categorized as coastal deposits, or lacustrine/estuarine. (TNO-GDN 2022. Velsen Bed; *TNO-GDN 2022. Wormer Member)*. So, they are on the boundary of fresh- and salt-water environments (fluvial – marine), often being brackish themselves (Pickett, 1982). Furthermore, the clear presence of shells and higher carbonate content of the layers indicate a strong biogenic production (van den Brenk & van Lil, 2020; van Lil & van den Brenk, 2021). High Rb to Sr ratios appear in the Velsen Bed and Wormer Member where greigite is present, but just as well in the Almere Bed, where there is none. Terrestrial input or OM availability and corresponding biogenic activity were thus not limiting factors preserving greigite in the Lake IJssel. Much of these observations seem comparable to the system observed in the Tisa section by Liu et al. (2017).

A further indication as to what might have been the limiting factor comes from core observations. Vivianite $(Fe_3(PO_4)_2 \cdot 8H_2O)$ is present in the clay sediments of the Velsen Bed and Wormer Member. Vivianite can occur in various geological environments, including fluvial, lacustrine, marine, estuarine, and waterlogged soils. It can precipitate in sediments under reducing conditions (Grizelj et al., 2017; McGowan1 & Prangnell, 2006; Nriagu, 1972; Rothe et al., 2016). The Velsen Bed and Wormer Member rank among these. The mineral's formation requires specific circumstances. High ferric iron, organic-rich conditions, as well as very low dissolved S^{2-} concentrations (Árpád et al., 2021; Dodd et al., 2000, 2003; Nriagu, 1972).

Based on these observations an interpretation comparable to the Tisa section can be made. Continental input and biological production were not limiting, since the Rb to Sr ratio are high in the greigite interval and calcite presence indicate biological activity. The presence of vivianite indicates high ferric iron and OM concentrations, which match with the previously stated interpretation. Furthermore, it also indicates very low sulfate concentrations, which could halt the reaction transforming greigite into pyrite: A mechanism similar to that of the Tisa section (Liu et al., 2017). The influx of riverine freshwater of the Oer-Vecht and Oer-IJssel lowers the sulfate concentration in the water, and limits the reaction (Berner, 1984), allowing the preservation of greigite.

Biological greigite forms well in these circumstances. However, as there are no strains of greigite MTB in pure culture, there is little known about how and under which conditions the bacteria synthesize greigite. Nonetheless, it can be argued that considering the anaerobic and sulfidic conditions in which they are found, biomineralization occurs only in the absence of oxygen (Bazylinski & Frankel, 2004). These circumstances fit well with the scenario presented above. Evidence that this occurred in the Lake IJssel remains insufficient.

Another point that can be gleaned from the data is the alternation in pyrite and greigite. These appear in separate layers, as well as combined. Van Baak et al. (2016) argue that the interchange of greigite and pyrite can be used as an environmental proxy. A larger presence of pyrite would indicate marine influences, while a larger greigite presence is indicative of freshwater input. An argument can be made that this hypothesis to some degree is applicable to the Lake IJssel. The thermomagnetic runs indicate that pyrite can be found in the Almere Bed, Flevomeer Bed, Hollandveen Member, Wormer Member, and Velsen Bed. All these layers have a brackish setting. Greigite only appears in the Wormer Member and Velsen Bed. These last two layers do feature more riverine input, and thus freshwater input. A point of critique on this hypothesis would be that sample 264 of the core VC26 (Fig. 13 C) contains only pyrite while being in the Wormer Member. This could mean that at that a point in time there was more marine influence, but to prove this more samples would likely need to be subjected to thermomagnetic analyses.

There are however still several points that can be added or improved upon in this research. While the data obtained in this study clearly points in the direction of greigite, a

more robust case could be made using supplementary methods. A further assessment of the magnetic domain state and the magnetic interactions can be made by creating first-order-reversal-curve (FORC) diagrams. This would allow for magnetic parameters and characteristics to be discerned which in turn could distinctly identify the magnetic minerals, and potentially whether they are biological in origin. The thermomagnetic run results show a point of interest too, untouched in this research. Thermomagnetic runs of VC15: 20, 333, 354, 405 (Fig. 11 B, C, D, E) VC17: 874 (Fig. 12 C), and VC26: 264 (Fig. 13 C), all show an increase in magnetization starting at temperatures of about 120 degrees Celsius. This is past the water evaporation temperature, and thus could be a magnetic mineral. Low temperature thermomagnetic runs should be performed to elucidate the origin of this magnetization optimum.

4.3 Curvy-Linear magnetic anomalies

In order to explain the magnetic lineations, a closer look is necessary at the stratigraphy. As was concluded in the previous paragraph, the magnetic signal finds its origin in the layers belonging to the Velsen Bed and the Wormer Member. In VC15, VC17, and VC26 these strata, or parts of them, are present. These cores all feature an anomaly too, either positive or negative. When looking at the stratigraphy of cores VC13, VC30, VC31, and VC32 (Fig. 5) it becomes apparent that an absence of these facies and their respective deposits leads to a less intense magnetic signal. The presence of the Velsen Bed and Wormer Member seems to be a prerequisite to forming a magnetic anomaly. Positive and negative anomalies both indicate a similar magnetic signal, as is illustrated by the presence of greigite in both VC15 and VC26, and are a result of the filtering method used by van den Brenk & van Lil (2020), and van Lil & van den Brenk (2021). A potential flaw in this explanation is that the magnetism found in core VC17 is weak in comparison to cores VC15 and VC26. Yet it is indicated as a relatively strong magnetic anomaly (Fig. 5). A possible explanation for this could be that the core simply did not reach deep enough to exhume the relevant strata. Considering the lithology of the core, it could very well be that the Velsen Bed and Wormer Member can be found deeper in the subsurface. Greigite can thus be formed in the stratigraphic members that are the Wormer Member and the Velsen Bed. In the Lake IJssel region, these are primarily deposited in riverine settings at the interface of sea and river, over time allowing the creation of a linear magnetic anomaly, as sea levels rose.

Due to the way in which the ship-tow magnetic data is processed both positive and negative anomalies indicate a magnetic presence. It is unclear however what causes the switch between positive and negative anomaly. A further point of research could be to measure a core showcasing a neutral magnetization and containing the Velsen Bed and Wormer Member.

4.4 Paleomagnetic directions and intensity
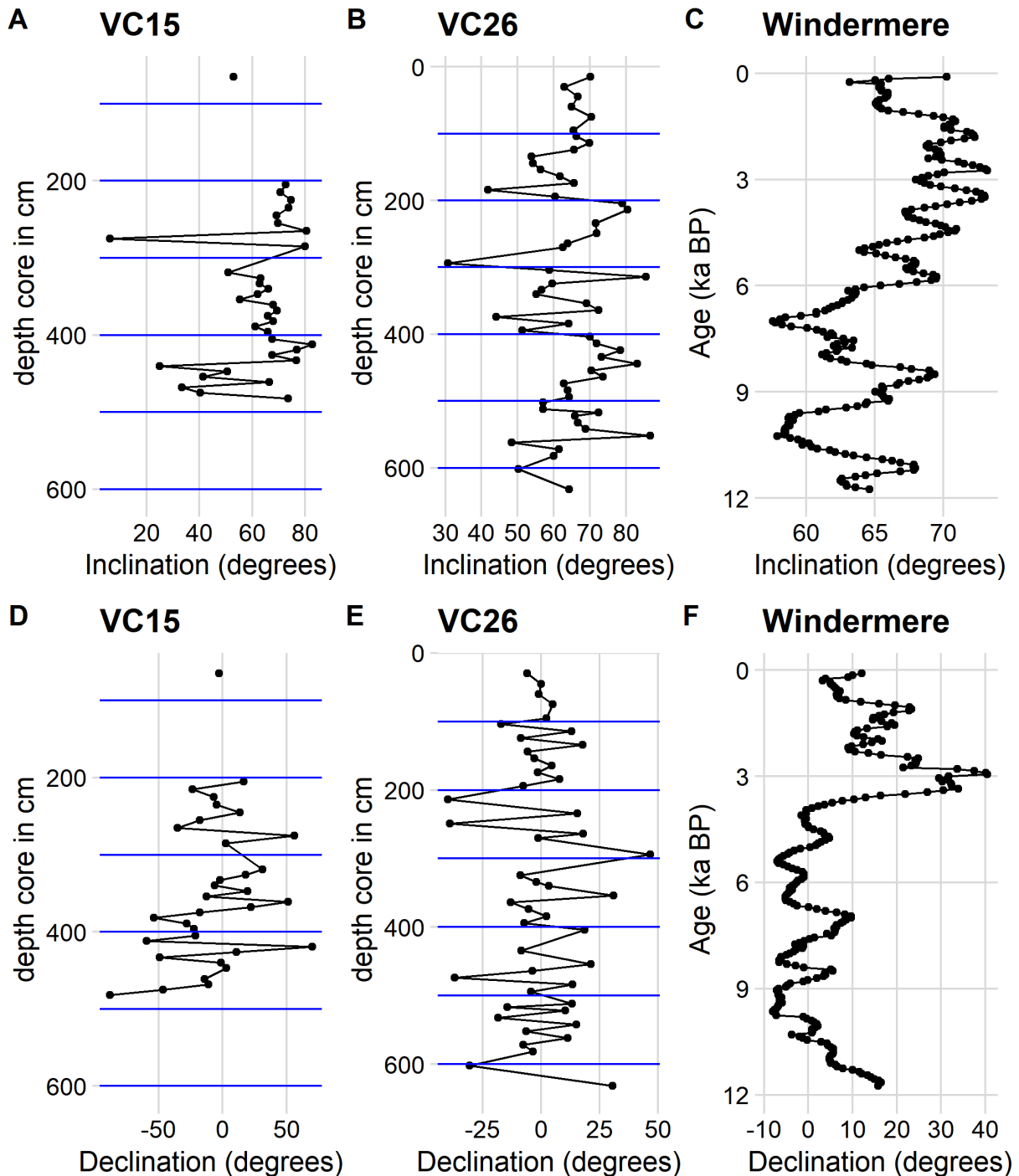
Figure 22: NRM directions of core VC15 and VC26 (A, B, D, E) compared to the UK master curve (C, F). Blue lines indicate core separate core segments.

In figure 22 the inclination and declination records are shown of the cores VC15 and VC26. Results of core VC17 are omitted since data points were too few. In order to compare the records a calibration curve is plotted (figure 22 C, F) (Avery et al., 2020) from Windermere in the UK, which is an update to the Paleo Secular Variation (PSV) master curve of Snowball & Thompson, 1990. Note that the depths of the cores do not relate with each other or with the age of the master curve. Remarkable are the differences in magnitude of the declination and

inclination between the cores and the calibration curve. The inclination trends of VC15 and VC26 feature an amplitude several tens of degrees larger than the master curve (Fig. 22 A, B, C). A possible explanation for this behavior could be drilling, or coring, induced remanent magnetization. Weaver et al. (1998) bring forward that mechanical disturbance of sediments during the coring process, in the presence of the magnetic field of the barrel of the core might induce magnetization. However, a different coring method was used in the Lake IJssel research.

The fact that the formations found in the Lake IJssel and spread throughout the Netherlands are spatially diachronic warrants the need for a dating method capable of correlating the different sections were these formations may be found. PSV is such a dating method. Comparing the graphs is difficult, as tie points lack. But the consecutive record of primarily VC26 (Fig. 22 B, E) shows that there is potential for matching with the master curve (Fig. 22 C, F) between the inclination and declination trends. VC15 (Fig. 22 A, D) might show similarities to VC26 in both inclination and declination, but these are less clear. However, considering the density of the data, and lack of dated calibration points, as of yet age correlation remains curve-wiggling. A direct contribution to PSV data sets of the Holocene in western Europe cannot be made yet, and further correlation with other sections in the Netherlands cannot be made with only the data of this research. In combination with other dating methods, such as carbon 14 dating, a calibration can be performed, and the data can be of use to correlate the different layers found in the Lake IJssel and the Netherlands.

A slope paleointensity record was created of the different cores (Fig. 23), and plotted alongside a comparative relative paleointensity curve generated by the PFM9K.1B model (Nilsson et al., 2014) on the location of the Lake IJssel, spanning the last 7 ka BP. Note that the depth of the cores does not correlate with the age of the comparative curve. While a direct comparison is not possible due to the different parameters being plotted, a comparison of trends could be. The trend visible in the PFM9K.1B model (Fig. 23 D) shows some resemblance to the trend visible in the interval of 0 - 350 cm of core VC26 (Fig. 23 C), but additional data points would be required to prove this. Between the cores themselves correlation is difficult too, as the depths do not correlate and data density is limited. Especially cores VC15 (Fig. 23 A) and VC17 (Fig. 23 B) have little data density. Improvements to create a full record could be made by taking more samples.
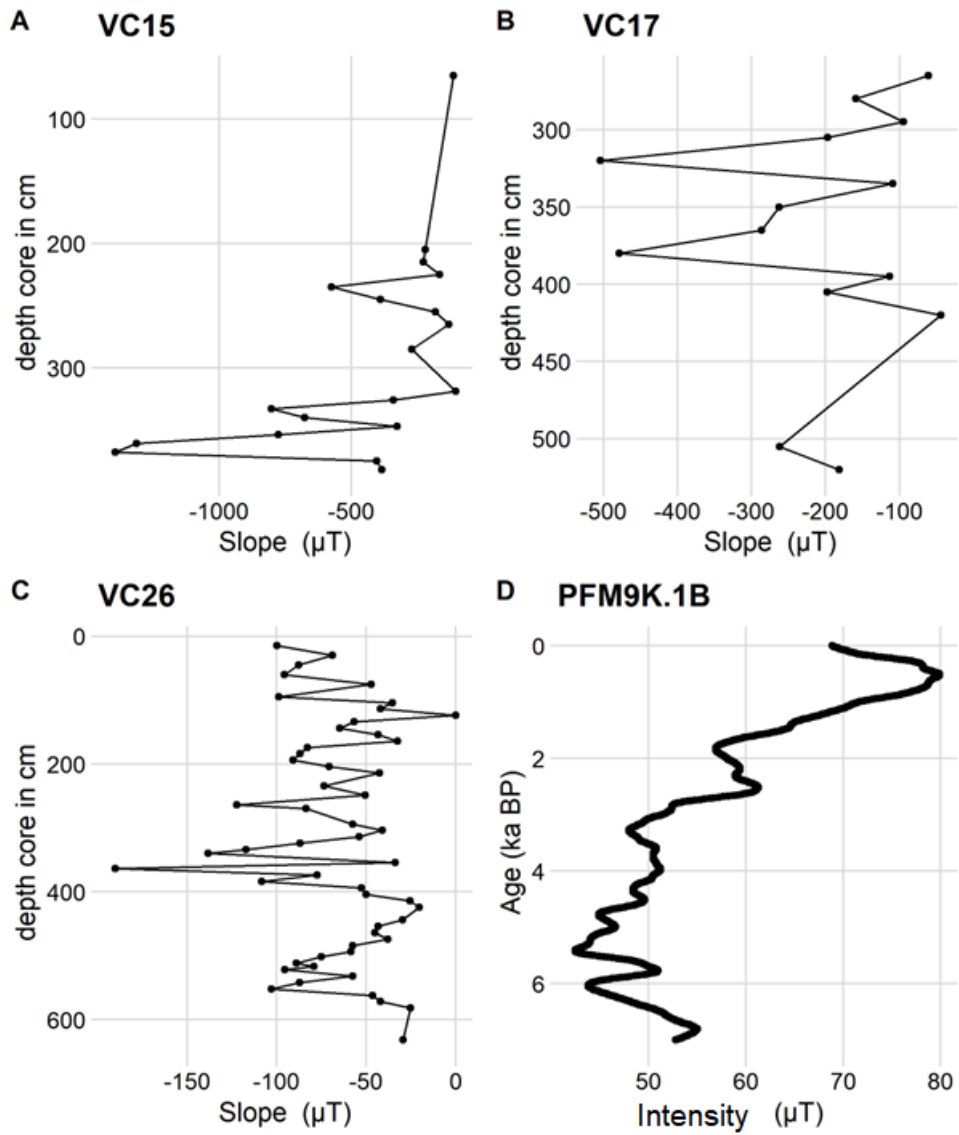
Figure 23: Slopes of the relative paleointensity record of cores VC15, VC17, VC26 and a model generated dataset of the Lake IJssel by the PFM9K.1B model (Nilsson et al., 2014).

5. Conclusions

The curvy magnetic lineations found in the Lake IJssel are created by greigite populations, primarily diagenetic and possibly biological in origin, formed in the Velsen Bed and Wormer Member. These layers are deposited at the interface of river and sea, creating a linear magnetic anomaly as the sea level rose. Both a positive as well as a negative anomaly are argued to be due to the presence of greigite. Circumstances allow for a biological origin of greigite, however the results are insufficient prove this origin. Additional research with use of FORC diagrams should enlighten more about the mineralogical origin of the greigite in the Lake IJssel lineations. The PSV results are indicative of a potential for the method to be used in dating the stratigraphic units of the Lake IJssel and in the Netherlands. With the addition of more datapoints to heighten data density, and absolutely dated tie points a relative and local time scale could be constructed.

6. References

Árpád, C., Lajos, P., Ferenc, K., Sándor, S., & Péter, R. (2021). Vivianite formation as indicator of human impact in porous sediments. Environmental Earth Sciences, 80(17), 558. https://doi.org/10.1007/s12665-021-09866-2

Avery, R. S., Xuan, C., Kemp, A. E. S., Bull, J. M., Cotterill, C., Fielding, J. J., Pearce, R. B., & Croudace, I. W. (2020). Paleosecular geomagnetic variation for the Holocene measured from U-channels 2014-2016 [Data set]. In University of Southampton. PANGAEA.

Avery, R. S., Xuan, C., Kemp, A. E. S., Bull, J. M., Cotterill, C., Fielding, J. J., Pearce, R. B., & Croudace, I. W. (2020). Paleosecular geomagnetic variation for the Holocene measured from U-channels 2014-2016 [Data set]. In University of Southampton. PANGAEA. https://doi.org/10.1594/PANGAEA.917458

Bazylinski, D. A., & Frankel, R. B. (2004). Magnetosome formation in prokaryotes. Nature Reviews Microbiology, 2(3), 217–230.

Beets, D.J. & Van der Spek, A.F., 2000. The Holocene evolution of the barrier and back barrier basins of Belgium and the Netherlands as a function of relative sea level rise, late Weichselian morphology and sediment supply. Netherlands Journal of Geosciences 79: 3-16.

Beets, D.J., Roep, Th .B. & Westerhoff , W.E., 1996. The Holocene Bergen Inlet: Closing history and related barrier progradation. In: D.J. Beets et al. (Eds): Coastal studies on the Holocene of the Netherlands. Mededelingen Rijks Geologische Dienst 57: 97-113.

Beets, D.J., Van der Spek, A.J.F. & Van der Valk, L., 1994. Holocene ontwikkeling van de Nederlandse kust. Report no. 40.016, Rijks Geologische Dienst, Haarlem: 1-53

Béguin, A., Filippidi, A., de Lange, G. J., & de Groot, L. V. (2019). The evolution of the Levantine Iron Age geomagnetic Anomaly captured in Mediterranean sediments. Earth and Planetary Science Letters, 511, 55–66. https://doi.org/10.1016/j.epsl.2019.01.021

Béguin, A., Paterson, G. A., Biggin, A. J., & Groot, L. V. (2020). Paleointensity.org: An Online, Open Source, Application for the Interpretation of Paleointensity Data. Geochemistry, Geophysics, Geosystems, 21(5). https://doi.org/10.1029/2019GC008791

Bennema, J. 1954. Bodem- en zeespiegelbewegingen in het Nederlandse kustgebied. PhD Thesis, Wageningen University, 85 p.

Berendsen, H. J. A. (2005). Landschappelijk Nederland: De fysisch-geografische regio's. Koninklijke Van Gorcum; /z-wcorg/.

Berner, R. A. (1984). Sedimentary pyrite formation: An update. Geochimica et Cosmochimica Acta, 48(4), 605–615. https://doi.org/10.1016/0016-7037(84)90089-9

Blanchet, C. L., Thouveny, N., & Vidal, L. (2009). Formation and preservation of greigite (Fe3S4) in sediments from the Santa Barbara Basin: Implications for paleoenvironmental changes during the past 35 ka. Paleoceanography, 24(2).

Bos, I.J., 2010. Distal Delta-Plain Successions. Architecture and Lithofacies of Lake Fills and Organics in the Holocene Rijn–Maas Delta, The Netherlands. Ph.D. thesis, Utrecht University: 208 pp.

Busschers, F.S., 2008. Unravelling the Rhine. Response of a Fluvial System to Climate Change, Sea-Level Oscillation and Glaciation. Ph.D. thesis, Vrije Universiteit, Amsterdam.

Byrne, J. M., Klueglein, N., Pearce, C., Rosso, K. M., Appel, E., & Kappler, A. (2015). Redox cycling of Fe (II) and Fe (III) in magnetite by Fe-metabolizing bacteria. Science, 347(6229), 1473–1476.

Carlson, A. E., & Clark, P. U. (2012). Ice sheet sources of sea level rise and freshwater discharge during the last deglaciation. Reviews of Geophysics, 50(4), RG4007. https://doi.org/10.1029/2011RG000371

Chang, L., Vasiliev, I., van Baak, C., Krijgsman, W., Dekkers, M. J., Roberts, A. P., Gerald, J. D. F., van Hoesel, A., & Winklhofer, M. (2014). Identification and environmental interpretation of diagenetic and biogenic greigite in sediments: A lesson from the Messinian Black Sea. Geochemistry, Geophysics, Geosystems, 15(9), 3612–3627. https://doi.org/10.1002/2014GC005411

Chang, L., Winklhofer, M., Roberts, A. P., Heslop, D., Florindo, F., Dekkers, M. J., Krijgsman, W., Kodama, K., & Yamamoto, Y. (2013). Low-temperature magnetic properties of pelagic carbonates: Oxidation of biogenic magnetite and identification of magnetosome chains. Journal of Geophysical Research: Solid Earth, 118(12), 6049–6065.

Chen, J., An, Z., & Head, J. (1999). Variation of Rb/Sr Ratios in the Loess-Paleosol Sequences of Central China during the Last 130,000 Years and Their Implications for Monsoon Paleoclimatology. Quaternary Research, 51(3), 215–219. https://doi.org/10.1006/qres.1999.2038

Collinson, D. W. (1983). Methods in Rock Magnetism and Palaeomagnetism. Springer Netherlands. https://doi.org/10.1007/978-94-015-3979-1

Da Silva, A.-C., Dekkers, M. J., Mabille, C., & Boulvain, F. (2012). Magnetic susceptibility and its relationship with paleoenvironments, diagenesis and remagnetization: Examples from the Devonian carbonates of Belgium. Studia Geophysica et Geodaetica, 56(3), 677–704. https://doi.org/10.1007/s11200-011-9005-9

Dankers, P. H. M., & Zijderveld, J. D. A. (1981). Alternating field demagnetization of rocks, and the problem of gyromagnetic remanence. Earth and Planetary Science Letters, 53(1), 89–92. https://doi.org/10.1016/0012-821X(81)90029-7

de Groot, L. V., Biggin, A. J., Dekkers, M. J., Langereis, C. G., & Herrero-Bervera, E. (2013). Rapid regional perturbations to the recent global geomagnetic decay revealed by a new Hawaiian record. Nature Communications, 4(1), 2727. https://doi.org/10.1038/ncomms3727

Dekkers, M. J. (1997). Environmental magnetism: An introduction. Geologie En Mijnbouw (Geology and Mining), 76(1/2), 163–182. https://doi.org/10.1023/A:1003122305503

Dekkers, M. J., Passier, H. F., & Schoonen, M. A. (2000). Magnetic properties of hydrothermally synthesized greigite (Fe 3 S 4)—II. High-and low-temperature characteristics. Geophysical Journal International, 141(3), 809–819.

Dodd, J., Large, D. J., Fortey, N. J., Kemp, S., Styles, M., Wetton, P., & Milodowski, A. (2003). Geochemistry and petrography of phosphorus in urban canal bed sediment. Applied Geochemistry, 18(2), 259–267. https://doi.org/10.1016/S0883-2927(02)00124-5

Dodd, J., Large, D. J., Fortey, N. J., Milodowski, A. E., & Kemp, S. (2000). A Petrographic Investigation of two Sequential Extraction Techniques Applied to Anaerobic Canal Bed Mud. Environmental Geochemistry and Health, 22(4), 281–296. https://doi.org/10.1023/A:1006743630918

Doppert, J.W.Chr., Ruegg, G.H.J., Van Staalduinen, C.J., Zagwijn, W.H., Zandstra, J.G. 1975. Formaties van het Kwartair en Boven-Tertiair in Nederland. In: Zagwijn, W.H., Van Staalduinen, C.J. (eds.): Toelichting bij geologische overzichtskaarten van Nederland. Rijks Geologische Dienst, Haarlem, 11-56.

Dunlop, D. J., & Özdemir, Ö. (1997). Rock Magnetism: Fundamentals and Frontiers (1st ed.). Cambridge University Press. https://doi.org/10.1017/CBO9780511612794

Egli, R. (2004). Characterization of Individual Rock Magnetic Components by Analysis of Remanence Curves, 1. Unmixing Natural Sediments. Studia Geophysica et Geodaetica, 48(2), 391–446. https://doi.org/10.1023/B:SGEG.0000020839.45304.6d

Ente, P.J., 1986. Het ontstaan van het Marsdiep en de Zuiderzee. Lezing gehouden te Amsterdam op 25-3-1983, met aanvullingen. Werkdocument no. 1986-102abw. Rijksdienst voor de IJsselmeerpolders, Lelystad: 22 p

Evans, M. E., & Heller, F. (2003). Environmental magnetism principles and applications of enviromagnetics. Academic Press. http://www.sciencedirect.com/science/publication?issn=00746142&volume=86

Fabian, K., Shcherbakov, V. P., & McEnroe, S. A. (2013). Measuring the Curie temperature: MEASURING THE CURIE TEMPERATURE. Geochemistry, Geophysics, Geosystems, 14(4), 947–961. https://doi.org/10.1029/2012GC004440

Farina, M., Esquivel, D. M. S., & de Barros, H. G. (1990). Magnetic iron-sulphur crystals from a magnetotactic microorganism. Nature, 343(6255), 256–258.

Frankel, R. B., & Bazylinski, D. A. (2006). How magnetotactic bacteria make magnetosomes queue up. Trends in Microbiology, 14(8), 329–331.

Frankel, R. B., Blakemore, R. P., Torres de Araujo, F. F., Esquivel, D. M. S., & Danon, J. (1981). Magnetotactic bacteria at the geomagnetic equator. Science, 212(4500), 1269–1270.

Fu, Y., von Dobeneck, T., Franke, C., Heslop, D., & Kasten, S. (2008). Rock magnetic identification and geochemical process models of greigite formation in Quaternary marine sediments from the Gulf of Mexico (IODP Hole U1319A). Earth and Planetary Science Letters, 275(3–4), 233–245. https://doi.org/10.1016/j.epsl.2008.07.034

Grizelj, A., Bakrač, K., Horvat, M., Avanić, R., & Hećimović, I. (2017). Occurrence of vivianite in alluvial Quaternary sediments in the area of Sesvete (Zagreb, Croatia). Geologia Croatica, 70(1), 0–0.

Grommé, C. S., Wright, T. L., & Peck, D. L. (1969). Magnetic properties and oxidation of iron-titanium oxide minerals in Alae and Makaopuhi Lava Lakes, Hawaii. Journal of Geophysical Research, 74(22), 5277–5293. https://doi.org/10.1029/JB074i022p05277

Heslop, D., McIntosh, G., & Dekkers, M. J. (2004). Using time- and temperature-dependent Preisach models to investigate the limitations of modelling isothermal remanent magnetization acquisition curves with cumulative log Gaussian functions. Geophysical Journal International, 157(1), 55–63. https://doi.org/10.1111/j.1365-246X.2004.02155.x

Heslop, D., & Roberts, A. P. (2016). Analyzing paleomagnetic data: To anchor or not to anchor? Journal of Geophysical Research: Solid Earth, 121(11), 7742–7753. https://doi.org/10.1002/2016JB013387

Heslop, D., Roberts, A. P., Chang, L., Davies, M., Abrajevitch, A., & De Deckker, P. (2013). Quantifying magnetite magnetofossil contributions to sedimentary magnetizations. Earth and Planetary Science Letters, 382, 58–65.

Hijma, M.P. & Cohen, K.M., 2011. Holocene transgression of the Rijn river mouth area, The Netherlands/Southern North Sea: palaeogeography and sequence stratigraphy. Sedimentology 58: 1453-1485.

Jelgersma, S., 1966. Holocene sea-level changes during the last 10,000 years. Proc. Int. Symp. World Climate from 8000 to 0 BC. Royal Meteorological Society, London: 54-71.

Johnson, C. L., & McFadden, P. (2015). The Time-Averaged Field and Paleosecular Variation. In Treatise on Geophysics (pp. 385–417). Elsevier. https://doi.org/10.1016/B978-0-444-53802-4.00105-6

Kao, S.-J., Horng, C.-S., Roberts, A. P., & Liu, K.-K. (2004). Carbon–sulfur–iron relationships in sedimentary rocks from southwestern Taiwan: Influence of geochemical environment on greigite and pyrrhotite formation. Chemical Geology, 203(1), 153–168. https://doi.org/10.1016/j.chemgeo.2003.09.007

Kelder, N. A., Sant, K., Dekkers, M. J., Magyar, I., van Dijk, G. A., Lathouwers, Y. Z., Sztanó, O., & Krijgsman, W. (2018). Paleomagnetism in Lake Pannon: Problems, Pitfalls, and Progress in Using Iron Sulfides for Magnetostratigraphy. Geochemistry, Geophysics, Geosystems, 19(9), 3405–3429. https://doi.org/10.1029/2018GC007673

Kiden, P., Denys, L. & Johnston, P., 2002. Late Quaternary sea-level change and isostatic and tectonic land movements along the Belgian-Dutch North Sea coast: Geological data and model results. Journal of Quaternary Science 17: 535-546.

Kirschvink, J. L., & Chang, S.-B. R. (1984). Ultrafine-grained magnetite in deep-sea sediments: Possible bacterial magnetofossils. Geology, 12(9), 559–562.

Klumpp, S., Lefèvre, C. T., Bennet, M., & Faivre, D. (2019). Swimming with magnets: From biological organisms to synthetic devices. Physics Reports, 789, 1–54.

Koymans, M. R., Langereis, C. G., Pastor-Galán, D., & van Hinsbergen, D. J. J. (2016). Paleomagnetism.org: An online multi-platform open source environment for paleomagnetic data analysis. Computers & Geosciences, 93, 127–137. https://doi.org/10.1016/j.cageo.2016.05.007

Kruiver, P. P., & Passier, H. F. (2001). Coercivity analysis of magnetic phases in sapropel S1 related to variations in redox conditions, including an investigation of the S ratio. Geochemistry, Geophysics, Geosystems, 2(12). https://doi.org/10.1029/2001GC000181

Kruiver, P. P., Dekkers, M. J., & Heslop, D. (2001). Quantification of magnetic coercivity components by the analysis of acquisition curves of isothermal remanent magnetisation. Earth and Planetary Science Letters, 189(3–4), 269–276. https://doi.org/10.1016/S0012-821X(01)00367-3

Lajos, P., Ferenc, K., Sándor, S., & Péter, R. (2021). Vivianite formation as indicator of human impact in porous sediments. Environmental Earth Sciences, 80(17), 558. https://doi.org/10.1007/s12665-021-09866-2

Lenselink, G. & Koopstra, R., 1994. Ontwikkeling in het Zuiderzeegebied; van Meer Flevo, via de Almere-lagune, tot Zuiderzee. In: Rappol, M. & Soonius, C.M. (Eds.): In de Bodem van Noord-Holland. Lingua Terrae, Amsterdam:129- 140.

Liu, S., Krijgsman, W., Dekkers, M. J., & Palcu, D. (2017). Early diagenetic greigite as an indicator of paleosalinity changes in the middle Miocene Paratethys Sea of central Europe: EARLY DIAGENETIC GREIGITE IN PARATETHYS. Geochemistry, Geophysics, Geosystems, 18(7), 2634–2645. https://doi.org/10.1002/2017GC006988

Luo, G., Richoz, S., van de Schootbrugge, B., Algeo, T. J., Xie, S., Ono, S., & Summons, R. E. (2018). Multiple sulfur-isotopic evidence for a shallowly stratified ocean following the Triassic-Jurassic boundary mass extinction. Geochimica et Cosmochimica Acta, 231, 73–87. https://doi.org/10.1016/j.gca.2018.04.015

Mann, S., Sparks, N. H., Frankel, R. B., Bazylinski, D. A., & Jannasch, H. W. (1990). Biomineralization of ferrimagnetic greigite (Fe3S4) and iron pyrite (FeS2) in a magnetotactic bacterium. Nature, 343(6255), 258–261.

McGowan1, G., & Prangnell, J. (2006). The significance of vivianite in archaeological settings. Geoarchaeology: An International Journal, 21(1), 93–111.

McNeill, D. F., Ginsburg, R. N., Chang, S.-B. R., & Kirschvink, J. L. (1988). Magnetostratigraphic dating of shallow-water carbonates from San Salvador, Bahamas. Geology, 16(1), 8. https://doi.org/10.1130/0091-7613(1988)016<0008:MDOSWC>2.3.CO;2

Mullender, T. A. T., Frederichs, T., Hilgenfeldt, C., de Groot, L. V., Fabian, K., & Dekkers, M. J. (2016). Automated paleomagnetic and rock magnetic data acquisition with an in-line horizontal "2G" system: AUTOMATED MAGNETIC DATA ACQUISITION. Geochemistry, Geophysics, Geosystems, 17(9), 3546–3559. https://doi.org/10.1002/2016GC006436

Mullender, T. a. T., van Velzen, A. J., & Dekkers, M. J. (1993). Continuous drift correction and separate identification of ferrimagnetic and paramagnetic contributions in thermomagnetic runs. Geophysical Journal International, 114(3), 663–672. https://doi.org/10.1111/j.1365-246X.1993.tb06995.x

Nilsson, A., Holme, R., Korte, M., Suttie, N., & Hill, M. (2014). Reconstructing Holocene geomagnetic field variation: New methods, models and implications. Geophysical Journal International, 198(1), 229–248. https://doi.org/10.1093/gji/ggu120

Nriagu, J. O. (1972). Stability of vivianite and ion-pair formation in the system fe3(PO4)2-H3PO4H3PO4-H2o. Geochimica et Cosmochimica Acta, 36(4), 459–470. https://doi.org/10.1016/0016-7037(72)90035-X

Oost, A.P., De Haas, H., IJnsen, F., Van den Boogert, J.M. & De Boer, P.L., 1993. The 18.6 Year nodal cycle and its impact on tidal sedimentation. Sedimentary Geology 87: 1-11.

Passier, H. F., de Lange, G. J., & Dekkers, M. J. (2001). Magnetic properties and geochemistry of the active oxidation front and the youngest sapropel in the eastern Mediterranean Sea. Geophysical Journal International, 145(3), 604–614. https://doi.org/10.1046/j.0956-540x.2001.01394.x

Peters, C., & Thompson, R. (1998). Magnetic identification of selected natural iron oxides and sulphides. Journal of Magnetism and Magnetic Materials, 183(3), 365–374.

Pickett, T. E. (1982). Lagoonal Sedimentation. In M. Schwartz, Beaches and Coastal Geology (pp. 505–505). Springer US. https://doi.org/10.1007/0-387-30843-1_251

Pons, L.J. & Wiggers, A.J., 1960. De holocene wordingsgeschiedenis van Noordholland en het Zuiderzeegebied; deel 2. Tijdschrift Koninklijk Nederlands Aardrijkskundig Genootschap, Tweede Reeks, 77: 3-57.

Pósfai, M., Cziner, K., MÁRTON, E., Márton, P., Buseck, P. R., Frankel, R. B., & Bazylinski, D. A. (2001). Crystal-size distributions and possible biogenic origin of Fe sulfides. European Journal of Mineralogy, 13(4), 691–703.

Robert A. Berner, Timothy Baldwin,. (1979). Authigenic Iron Sulfides as Paleosalinity Indicators. SEPM Journal of Sedimentary Research, Vol. 49. https://doi.org/10.1306/212F7923-2B24-11D7-8648000102C1865D

Roberts, A. P., & Weaver, R. (2005). Multiple mechanisms of remagnetization involving sedimentary greigite (Fe3S4). Earth and Planetary Science Letters, 231(3–4), 263–277.

Roberts, A. P., Chang, L., Rowan, C. J., Horng, C.-S., & Florindo, F. (2011a). Magnetic properties of sedimentary greigite (Fe3S4): An update. Reviews of Geophysics, 49(1). https://doi.org/10.1029/2010RG000336

Roberts, A. P., Chang, L., Rowan, C. J., Horng, C.-S., & Florindo, F. (2011b). Magnetic properties of sedimentary greigite (Fe 3 S 4): An update. Reviews of Geophysics, 49(1), RG1002. https://doi.org/10.1029/2010RG000336

Roberts, A. P., Reynolds, R. L., Verosub, K. L., & Adam, D. P. (1996). Environmental magnetic implications of greigite (Fe3S4) formation in a 3 my lake sediment record from Butte Valley, northern California. Geophysical Research Letters, 23(20), 2859–2862.

Robertson, D. J., & France, D. E. (1994). Discrimination of remanence-carrying minerals in mixtures, using isothermal remanent magnetisation acquisition curves. Physics of the Earth and Planetary Interiors, 82(3–4), 223–234. https://doi.org/10.1016/0031-9201(94)90074-4

Roep, T.B., Beets, D.J. & De Jong, J., 1979. Het zeegat tussen Alkmaar en Bergen van ca. 1900 tot 1300 jaar v. Chr. Alkmaarse Historische Reeks, deel III: 9–35.

Rothe, M., Kleeberg, A., & Hupfer, M. (2016). The occurrence, identification and environmental relevance of vivianite in waterlogged soils and aquatic sediments. Earth-Science Reviews, 158, 51–64.

Rowan, C. J., Roberts, A. P., & Broadbent, T. (2009). Reductive diagenesis, magnetite dissolution, greigite growth and paleomagnetic smoothing in marine sediments: A new view. Earth and Planetary Science Letters, 277(1), 223–235. https://doi.org/10.1016/j.epsl.2008.10.016

Sagnotti, L., Cascella, A., Ciaranfi, N., Macrì, P., Maiorano, P., Marino, M., & Taddeucci, J. (2010). Rock magnetism and palaeomagnetism of the Montalbano Jonico section (Italy): Evidence for late diagenetic growth of greigite and implications for magnetostratigraphy. Geophysical Journal International, 180(3), 1049–1066.

Sant, K., Mandic, O., Rundić, L., Kuiper, K. F., & Krijgsman, W. (2018). Age and evolution of the Serbian Lake System: Integrated results from Middle Miocene Lake Popovac. Newsletters on Stratigraphy, 51(1), 117–143. https://doi.org/10.1127/nos/2016/0360

Sm_30. (n.d.). Retrieved February 25, 2022, from http://www.zhinstruments.com/sm_30.html

Smith, D. E., Harrison, S., Firth, C. R., & Jordan, J. T. (2011). The early Holocene sea level rise. Quaternary Science Reviews, 30(15–16), 1846–1860. https://doi.org/10.1016/j.quascirev.2011.04.019

Snowball, I. F. (1997). Gyroremanent magnetization and the magnetic properties of greigite-bearing clays in southern Sweden. Geophysical Journal International, 129(3), 624–636. https://doi.org/10.1111/j.1365-246X.1997.tb04498.x

Snowball, I., & Thompson, R. (1990). A stable chemical remanence in Holocene sediments. Journal of Geophysical Research: Solid Earth, 95(B4), 4471–4479.

Stolz, J. F., Chang, S.-B. R., & Kirschvink, J. L. (1986). Magnetotactic bacteria and single-domain magnetite in hemipelagic sediments. Nature, 321(6073), 849–851. https://doi.org/10.1038/321849a0

Stouthamer, E., , Cohen, K.M., Hoek, W.Z.,. (2015). De vorming van het land: Geologie en geomorfologie. /z-wcorg/.

Tauxe, L., Pick, T., & Kok, Y. S. (1995). Relative paleointensity in sediments: A Pseudo-Thellier Approach. Geophysical Research Letters, 22(21), 2885–2888. https://doi.org/10.1029/95GL03166

TNO-GDN (2022). Almere Laag. In: Stratigrafische Nomenclator van Nederland, TNO – Geologische Dienst Nederland. Geraadpleegd op 29-06-2022 op http://www.dinoloket.nl/stratigrafische-nomenclator/almere-laag.

TNO-GDN (2022). Boven-Noordzee Groep. In: Stratigrafische Nomenclator van Nederland, TNO – Geologische Dienst Nederland. Geraadpleegd op 21-04-2022 op http://www.dinoloket.nl/stratigrafische-nomenclator/boven-noordzee-groep.

TNO-GDN (2022). Flevomeer Laag. In: Stratigrafische Nomenclator van Nederland, TNO – Geologische Dienst Nederland. Geraadpleegd op 29-06-2022 op http://www.dinoloket.nl/stratigrafische-nomenclator/flevomeer-laag.

TNO-GDN (2022). Formatie van Boxtel. In: Stratigrafische Nomenclator van Nederland, TNO – Geologische Dienst Nederland. Geraadpleegd op 01-07-2022 op http://www.dinoloket.nl/stratigrafische-nomenclator/formatie-van-boxtel

TNO-GDN (2022). Formatie van Naaldwijk. In: Stratigrafische Nomenclator van Nederland, TNO – Geologische Dienst Nederland. Geraadpleegd op 29-06-2022 op http://www.dinoloket.nl/stratigrafische-nomenclator/formatie-van-naaldwijk.

TNO-GDN (2022). Gieten Member. In: Stratigraphic Nomenclature of the Netherlands, TNO – Geological Survey of the Netherlands. Accessed on 01-07-2022 from http://www.dinoloket.nl/en/stratigraphic-nomenclature/gieten-member.

TNO-GDN (2022). Hollandveen Laagpakket. In: Stratigrafische Nomenclator van Nederland, TNO – Geologische Dienst Nederland. Geraadpleegd op 29-06-2022 op http://www.dinoloket.nl/stratigrafische-nomenclator/hollandveen-laagpakket.

TNO-GDN (2022). Laag van Velsen. In: Stratigrafische Nomenclator van Nederland, TNO – Geologische Dienst Nederland. Geraadpleegd op 24-06-2022 op http://www.dinoloket.nl/stratigrafische-nomenclator/laag-van-velsen.

TNO-GDN (2022). Laag van Velsen. In: Stratigrafische Nomenclator van Nederland, TNO – Geologische Dienst Nederland. Geraadpleegd op 29-06-2022 op http://www.dinoloket.nl/stratigrafische-nomenclator/laag-van-velsen.

TNO-GDN (2022). Laagpakket van Walcheren. In: Stratigrafische Nomenclator van Nederland, TNO – Geologische Dienst Nederland. Geraadpleegd op 29-06-2022 op http://www.dinoloket.nl/stratigrafische-nomenclator/laagpakket-van-walcheren.

TNO-GDN (2022). Laagpakket van Wormer. In: Stratigrafische Nomenclator van Nederland, TNO – Geologische Dienst Nederland. Geraadpleegd op 29-06-2022 op http://www.dinoloket.nl/stratigrafische-nomenclator/laagpakket-van-wormer.

TNO-GDN (2022). Wormer Member. In: Stratigraphic Nomenclature of the Netherlands, TNO – Geological Survey of the Netherlands. Accessed on 24-06-2022 from http://www.dinoloket.nl/en/stratigraphic-nomenclature/wormer-member

TNO-GDN (2022). Zuiderzee Laag. In: Stratigrafische Nomenclator van Nederland, TNO – Geologische Dienst Nederland. Geraadpleegd op 29-06-2022 op http://www.dinoloket.nl/stratigrafische-nomenclator/zuiderzee-laag.

van Baak, C. G. C., Vasiliev, I., Palcu, D. V., Dekkers, M. J., & Krijgsman, W. (2016). A Greigite-Based Magnetostratigraphic Time Frame for the Late Miocene to Recent DSDP Leg 42B Cores from the Black Sea. Frontiers in Earth Science, 4. https://doi.org/10.3389/feart.2016.00060

Van de Plassche, O., 1982. Sea-level change and water-level movements in the Netherlands during the Holocene, Mededelingen Rijks Geologische Dienst 36 (1): 1-93.

van den Brenk, S., & van Lil, R. (2020). Inventariserend Veldonderzoek (opwaterfase) Magnetische lineaties en inventarisatie wrakresten IJsselmeer en Markermeer, 2019 en 2020 (No. 20A015-04; p. 91). Rijksdienst voor het Cultureel Erfgoed.

Van Den Brenk, S. & Van Lil, R. (2017). Zandwinning IJsselmeer, vaarweg VAL Urk-Den Oever, C en D vakken [Data set]. DANS Data Station Archaeology. https://doi.org/10.17026/DANS-285-DAQH Van der Molen, J. & De Swart, H.E., 2001. Holocene wave conditions and wave-induced sand transport in the southern North Sea. Journal of Geophysical Research 106, C5: 9339-9362.

Van der Spek, A., 1994a. Holocene depositional sequences in the Dutch Wadden Sea south of the island of Ameland, Large-Scale Evolution of Holocene Tidal Basins in the Netherlands. Ph.D. thesis, University Utrecht: 29-73.

van Lil, R., & van den Brenk, S. (2021). Inventariserend Veldonderzoek (opwaterfase) Combinatie van de resultaten van booronderzoek met magnetische anomalieën en subbottom profiler opnamen (No. 1; 21A010-01). Rijksdienst voor het Cultureel Erfgoed.

Vasiliev, I., Dekkers, M. J., Krijgsman, W., Franke, C., Langereis, C. G., & Mullender, T. A. T. (2007). Early diagenetic greigite as a recorder of the palaeomagnetic signal in Miocene—Pliocene sedimentary rocks of the Carpathian foredeep (Romania). Geophysical Journal International, 171(2), 613–629. https://doi.org/10.1111/j.1365-246X.2007.03560.x

Vasiliev, I., Franke, C., Meeldijk, J. D., Dekkers, M. J., Langereis, C. G., & Krijgsman, W. (2008). Putative greigite magnetofossils from the Pliocene epoch. Nature Geoscience, 1(11), 782–786.

Vos, P. (2015). Origin of the Dutch Coastal Landscape: Long-Term Landscape Evolution of the Netherlands During the Holocene, Described and Visualized in National, Regional and Local Palaeogeographical Map Series. Barkhuis Publishing. http://ebookcentral.proquest.com/lib/uunl/detail.action?docID=5331749

Vos, P.C. & De Wolf, H., 1988. Paleo-ecologisch diatomeeën onderzoek in de Noordzee en provincie Noord-Holland in het kader van het kustgenese project, Taakgroep 5000. Report no. 500. Afdeling Paleobotanie Kenozoicum Diatomeeën, Rijks Geologische Dienst,Haarlem.

Vos, P.C. & De Wolf, H., 1993. Diatoms as a tool for reconstructing sedimentary environments in coastal wetlands; methodological aspects. Hydrobiologia 269/270: 285-296.

Walker, J. D. (2019). GSA Geologic Time Scale v. 5.0. Geological Society of America. https://doi.org/10.1130/2018.CTS005R3C

Weaver, P. P. E., Schmincke, H.-U., Firth, J. V., & Duffield, W. (Eds.). (1998). Proceedings of the Ocean Drilling Program, 157 Scientific Results (Vol. 157). Ocean Drilling Program. https://doi.org/10.2973/odp.proc.sr.157.1998

Weerts, H.J.T. 2003. Beschrijving lithostratigrafische eenheid. Nederlands Instituut voor Toegepaste Geowetenschappen TNO. Utrecht.

Westerhoff , W.E. & Dubelaar, W., 2012. Onder Nederland. Geologische Dienst Nederland TNO, Utrecht: 78 pp.

Westerhoff , W.E., De Mulder, E.F.J., De Gans, W., 1987. Toelichtingen bij de Geologische Kaart van Nederland 1:50.000; Bladen 19 W en 19 O (Alkmaar west en Alkmaar oost). Rijks Geologische Dienst, Haarlem.

Westerhoff, W.E., Wong, Th.E., De Mulder, E.F.J. 2003. Opbouw van de ondergrond. Deel 3. In: De Mulder, E.F.J., Geluk, M.C., Ritsema, I., Westerhoff, W.E., Wong, Th.E. (eds.): De ondergrond van Nederland. Netherlands Institute of Applied Geosciences TNO - National Geological Survey, 249-352.

Yamazaki, T. (2012). Paleoposition of the Intertropical Convergence Zone in the eastern Pacific inferred from glacial-interglacial changes in terrigenous and biogenic magnetic mineral fractions. Geology, 40(2), 151–154.

Yang, T., Dekkers, M. J., & Chen, J. (2018). Thermal Alteration of Pyrite to Pyrrhotite During Earthquakes: New Evidence of Seismic Slip in the Rock Record. Journal of Geophysical Research: Solid Earth, 123(2), 1116–1131. https://doi.org/10.1002/2017JB014973

Zagwijn, W.H., Van Staalduinen, C.J. (red.) 1975, Toelichting bij geologische overzichtskaarten van Nederland. Rijks Geologische Dienst, Haarlem.

Appendix A: Glossary Paleomagnetic Terms

- *Antiferromagnetic*: A magnetic structure in which two equal size ferromagnetic sublattices are aligned antiparallel, causing there to be no magnetic moment. Hematite is an example of this.
- *Curie temperature:* The distance between atoms increases with temperature, and thereby reduces the magnetic exchange interaction and thus magnetic moment. At the Curie temperature this magnetic exchange energy is overcome by the thermal energy and the individual magnetic moments of the atoms become independent. The material becomes paramagnetic.
- *Diamagnetic:* In a diamagnetic material all the spins of the electrons are paired. It has a negative susceptibility.
- *Ferrimagnetic:* A magnetic structure in which two unequal size ferromagnetic sublattices are aligned parallel to each other.
- *Ferromagnetic:* A magnetic structure where all atomic magnetic moments are aligned and are parallel.
- *Magnetic susceptibility:* A parameter expressing how easily a substance can be magnetized in a small applied magnetic field.
- *Magnetic remanence:* A magnetization that unlike 'induced magnetization' remains after removal of the applied magnetic field.
- *Magnetic saturation:* The highest level of magnetic moment a sample can reach. Further increase of the field strength does not result in a higher magnetic moment.
- *Multidomain:* When grain size increases, so does the magnetostatic energy of a magnetic particle. At a critical grain size threshold, the particle will begin to nucleate domain walls to minimize this energy. The particle is subsequently separated into multiple magnetic domains, of uniform magnetization but different direction.
- *Natural remanent magnetization (NRM):* The (natural) remanent magnetization present in a sample before any experiments are performed. It is a record of the Earth's magnetic field from when the mineral was formed or laid down in the sediments. Paleomagnetic methods can retrieve the original/primary NRM component and thus reconstruct the original position of the sample.
- *Néél temperature:* Often used as another term for Curie temperature, but meant to indicate the temperature at which the individual magnetic moments are aligned antiparallel to each other in antiferromagnetic substances.
- *Paramagnetic:* Materials that have individually behaving uncompensated electronic spins. A condition in which every free electron spin acts as an individual atomic magnet. When an external field is applied, these moment will align partially to said field, and at its removal so will the induced magnetic moment.
- *Single Domain:* A magnetic particle that is uniformly magnetized and has a single magnetic domain. Often grains are extremely small.

Appendix B: README

Appendix B contains a folder of the data files of the cores VC15, VC17, VC26 and excel files of the interpretations.